American Mineralogist, Volume 107, pages 1825–1839, 2022

Experimentally derived F, Cl, and Br fluid/melt partitioning of intermediate to silicic melts in shallow magmatic systems

Mike Cassidy[1,*,†], Alexander A. Iveson[2], Madeleine C.S. Humphreys[2], Tamsin A. Mather[1], Christoph Helo[3], Jonathan M. Castro[3], Philipp Ruprecht[4], David M. Pyle[1], and EIMF[5]

[1]Department of Earth Sciences, University of Oxford, South Parks Road, OX1 3AN, U.K.
[2]Department of Earth Science, University of Durham, Arthur Holmes Building, Science Site, South Road, Durham DH1 3LE, U.K.
[3]Institute for Geoscience, Johannes Gutenberg University of Mainz, J.-J.-Becher-Weg 21 D-55128 Mainz, Germany
[4]Department of Geological Sciences and Engineering, University of Nevada, South University, Reno, Nevada 89557, U.S.A
[5]Edinburgh Ion Microprobe Facility, Grant institute, The King's Buildings, James Hutton Road, Edinburgh EH9 3FE, U.K.

Abstract

The conditions under which halogens partition in favor of an exsolved fluid relative to the coexisting melt are key for understanding many magmatic processes, including volcanic degassing, evolution of crustal melt bodies, and ore formation. We report new F, Cl, and Br fluid/melt partition coefficients for intermediate to silicic melts, for which F and Br data are particularly lacking; and for varying CO_2-H_2O contents to assess the effects of changing fluid composition (X_{H_2O}) on Br fluid/melt partitioning for the first time. The experiments were conducted at pressures 50–120 MPa, temperatures 800–1100 °C, and volatile compositions [molar $X_{H_2O} = H_2O/(H_2O + CO_2)$] of 0.55 to 1, with redox conditions around the Nickel-Nickel Oxygen buffer ($f_{O_2} \approx$ NNO). Experiments were not doped with Cl, Br, or F and were conducted on natural crystal-bearing volcanic products at conditions close to their respective pre-eruptive state. The experiments therefore provide realistic constraints on halogen partitioning at naturally occurring, brine-undersaturated conditions. Measurements of Br, Cl, and F were made by Secondary Ion Mass Spectrometry (SIMS) on 13 experimental glass products spanning andesite to rhyolitic compositions, together with their natural starting materials from Kelud volcano, Indonesia, and Quizapu volcano, Chile. Fluid compositions were constrained by mass balance. Average bulk halogen fluid/melt partition coefficients and standard deviations are: $D_{Cl}^{fluid/melt} = 3.4$ (±3.7 1 s.d.), $D_{F}^{fluid/melt} = 1.7$ (±1.7), and $D_{Br}^{fluid/melt} = 7.1$ (±6.4) for the Kelud starting material (bulk basaltic andesite), and $D_{Cl}^{fluid/melt} = 11.1$ (±3.5), $D_{F}^{fluid/melt} = 0.8$ (±0.8), and $D_{Br}^{fluid/melt} = 31.3$ (±20.9) for Quizapu starting material (bulk dacite). The large range in average partition coefficients is a product of changing X_{H_2O}, pressure and temperature. In agreement with studies on synthetic melts, our data show an exponential increase of halogen $D^{fluid/melt}$ with increasing ionic radius, with partitioning behavior controlled by melt composition according to the nature of the complexes forming in the melt (e.g., SiF_4, NaCl, KBr). The fundamental chemistry of the different halogens (differing ionic size and electronegativities) controls the way in which partitioning responds to changes in melt composition and other variables. Experimental results confirm that more Cl partitions into the fluid at higher bulk Cl contents, higher melt Na, higher fluid X_{H_2O} ratios, and lower temperatures. Bromine shows similar behavior, though it seems to be more sensitive to temperature and less sensitive to Na content and X_{H_2O}. In contrast, F partitioning into the fluid increases as the melt silica content decreases (from 72 to 56 wt% SiO_2), which we attribute to the lower abundance of Si available to form F complexes in the melt. These new data provide more insights into the conditions and processes that control halogen degassing from magmas and may help to inform the collection and interpretation of melt inclusions and volcano gas data.

Keywords: Halogens, experiments, chlorine, fluorine, bromine, magma, volcanic gas; Experimental Halogens in Honor of Jim Webster

Introduction

Halogen behavior in magmas impacts a range of crustal processes, including magma evolution, degassing and ore mineralization, by influencing the physical and chemical properties of melts, fluids, and minerals (Aiuppa et al. 2009; Pyle and Mather 2009; Bodnar et al. 2013; Harlov and Aranovich 2018; Webster et al. 2018). Although halogens may partition into crystals, gases, and brine phases, this study concentrates on partitioning of halogens between the melt and aqueous fluid phase. Much previous work has concentrated on Cl, due to its ease of measurement in glasses by electron microprobe; and substantial advances in our understanding of Cl behavior in melts can be attributed to J.D. Webster. Chlorine fluid/melt partitioning ($D_{Cl}^{fluid/melt}$) behavior has been quantified for a range of silicate melt compositions (Webster and Holloway 1990; Webster 1997; Webster et al. 2014), pressures (Alletti et al. 2009; Botcharnikov et al. 2015;

* E-mail: michael.cassidy@earth.ox.ac.uk. Orcid 0000-0002-0658-2641
† Special collection papers can be found online at http://www.minsocam.org/MSA/AmMin/special-collections.html.

0003-004X/22/0010–1825$05.00/DOI: https://doi.org/10.2138/am-2022-8109

Webster et al. 2017), temperatures (Stelling et al. 2008), f_{O_2} (Beermann et al. 2015), and volatile contents (Lowenstern 1994; Botcharnikov et al. 2006; Alletti et al. 2009; Webster et al. 2014; Hsu et al. 2019; Chevychelov 2019). Fluorine, a relatively difficult element to measure in silicate glass (due to elemental interferences on the electron microprobe), has received less study, with most experiments focusing on end-member silicic or alkaline magmas (Fig. 1) (Webster and Holloway 1990; Borodulin et al. 2009; Iveson et al. 2017) and few data available for mafic and intermediate magmas (Chevychelov et al. 2008). Likewise, there are few data for bromine (Fig. 1) (Bureau et al. 2000, 2010; Cadoux et al. 2018) because of its low abundance and analytical challenges. Nonetheless, the behavior of bromine is of interest for its potential atmospheric impacts and detection of BrO in volcanic plumes by remote sensing (Aiuppa et al. 2005; Pyle and Mather 2009; Donovan et al. 2014; Gutmann et al. 2018).

The strong electronegativity of halogens largely controls their behavior in magmas and explains their propensity to form strong bonds, often with a high degree of polar or ionic character. The differing electronegativities and ionic radii of the halogens lead to element-specific effects in melts and fluids (Dolejš and Zajacz 2018; Webster et al. 2018). For instance, the high electronegativity of F (relative to Cl and Br) promotes strong interactions with cations in silicate melts, enhancing its solubility in melts and thus lowering its degassing potential compared to the other halogens (Webster et al. 2018). During crystallization of magmas, the relatively small F^- ion (1.33 Å) also substitutes effectively for similarly sized O^{2-} (1.26 Å) and OH^- (1.32–1.37 Å) within the melt and is therefore thought to partition into silicate melts during volatile-undersaturated magma differentiation (e.g., Dolejš and Baker 2007; Webster 1990). In contrast, Cl and Br are thought to become less enriched in the melt during differentiation, as they partition to a fluid phase as melts become more silicic. Their larger ionic masses and radii,

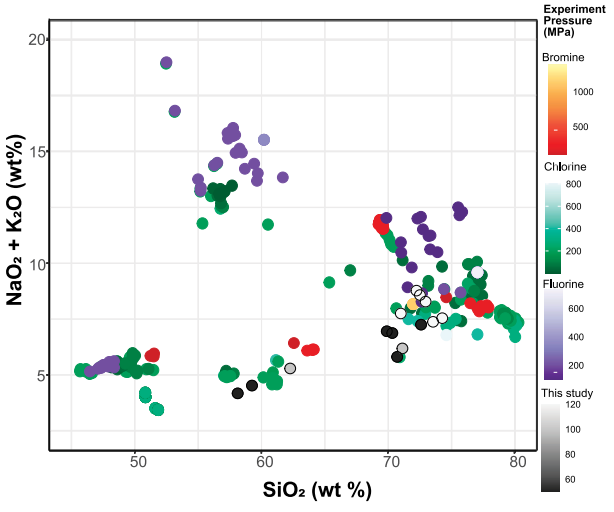

Figure 1. Total alkali silica plot for all the previous brine-undersaturated experiments, along with their corresponding pressures (MPa), for chlorine, fluorine, and bromine. The gray symbols represent the compositional space that the experiments in this study cover at pressures of 50 to 120 MPa. References for the data found in Online Materials[1] Table S1. (Color online.)

Cl^- (1.81 Å) and Br^- (1.95 Å), and the greater mismatch compared to O^{2-} and OH^- make Cl and Br less likely to be incorporated into the aluminosilicate network (Bureau et al. 2000) and promote a higher affinity with a coexisting aqueous fluid phase (Bureau et al. 2000; Bureau and Métrich 2003). Thus, Cl and Br fractionate more strongly into coexisting fluid during magmatic degassing compared with the lighter and smaller F (Teiber et al. 2014). Furthermore, the larger lattice energies for fluorides and higher hardness/bond strength as a ligand for complexing in comparison to chlorides means a preference of F for the melt and also the higher solubility of chlorides in aqueous fluids (Webster et al. 2015; Dolejš and Zajacz 2018).

The influence of melt composition on halogen behavior is a product of the complexes they form with the cations in the melt. Chlorine dominantly dissolves in the melt by complexation with network modifying alkaline earth metals (Mg, Ca), alkalis (Na, K), and also Al and Fe, whereas it dissolves as an HCl species in aqueous magmatic fluids (Webster 1997; Webster and De Vivo 2002; Thomas and Wood 2021). Conversely, it is thought that F occurs in silicate melts as Si-F, Al-F, Na-F, and Ca-F complexes (Dalou and Mysen 2015; Dalou et al. 2015; Bell and Simon 2011), while Br forms NaBr complexes at high pressure (>2 GPa) in hydrous felsic melts (Cochain et al. 2015; Louvel et al. 2020). The effect of melt composition on F and Br fluid/melt partitioning is currently unclear, as few studies span intermediate to silicic melt compositions (Fig. 1).

In magmatic systems the addition of volatiles such as CO_2 is known to influence the fluid/melt partitioning of chlorine: $D_{Cl}^{fluid/melt}$ decreases with increasing CO_2 addition, which is thought to be related to an increase of the activity coefficient for NaCl in the fluid phase, which decreases the stability of hydrated metal complexes in aqueous fluids, such as NaCl ion pairs (Alletti et al. 2009; Hsu et al. 2019). The effect of CO_2 on F and Br partitioning between fluid and melt is less studied, and our research assesses whether, like Cl, CO_2 presence in the fluid also decreases their fluid/melt partition coefficients. At low-Cl concentrations <2.5 wt% in basaltic melts (Webster et al. 2015) and <0.25 wt% in rhyolitic melts (Zajacz et al. 2012), Cl fluid/melt partitioning exhibits Henrian behavior, where the increasing Cl content of the melt varies linearly with increasing Cl in the coexisting fluid. However, with increasing Cl concentrations, partitioning behavior becomes non-linear, and subsolvus fluid exsolution yields a lower density aqueous phase and a higher density hydrosaline brine (e.g., Webster et al. 1999; Shinohara 2009). We concentrate here on brine-undersaturated conditions, where halogen partitioning should follow Henrian behavior and thus be more constant (Baker and Alletti 2012). These conditions apply to the many active magmatic systems that have low-halogen concentrations (Aiuppa et al. 2009) and lack a separate brine phase (Baker and Alletti 2012).

Recent experimental work by Thomas and Wood (2021) provides new insights into the chemical and thermodynamic basis for chlorine dissolution in silicate melts. The initial Cl dissolution into the melt involves the replacement of O^{2-} by two dissociated Cl^- ions:

$$Cl_2^{fluid} + (O^{2-})^{melt} = 2(Cl^-)^{melt} + 0.5O_2^{fluid\ or\ melt}$$

This leads to a formulation for chlorine solubility in anhydrous basalts (Thomas and Wood 2021):

$$\log(Cl^{melt}) = 0.984(64) - 930(70)P/T - 0.25\log(f_{O_2}) + 0.5\log(f_{Cl_2})$$

where P is in GPa, T in K, and f_{O_2} and f_{Cl_2} refer to the fugacities of a pure gas at 0.1 MPa and the temperature of interest. Values in parentheses are 1 standard error of the last two digits for the corresponding experimentally determined constants.

This relationship predicts that in mafic systems at fixed O_2 and Cl_2 fugacities, increasing temperature should increase chlorine solubility of the melt (and therefore lower $D_{Cl}^{fluid/melt}$), while increasing pressure should decrease the chlorine solubility (and thus increase $D_{Cl}^{fluid/melt}$). While the relationship between $D^{fluid/melt}$ with temperature has been observed experimentally for Cl and Br behaving in the same way (Webster et al. 2015; Cadoux et al. 2018), the results for F are less clear (Borodulin et al. 2009) and have been investigated in this study.

In this study, we test the theoretical and experimental hypotheses described above, i.e., the role of ionic size, metal-ligand complexing, volatile composition (H_2O-CO_2), and variable temperature, on fluid/melt partitioning of F, Cl, and Br. In particular, we present new data on andesitic to rhyolitic melts to test whether: (1) classic phase equilibria experiments can be used for halogen partitioning determination; (2) the larger Cl and Br ions behave similarly to each other, preferring the fluid over the melt with the fluid preference increasing with increasing ionic radius; (3) F partitions into melt during differentiation whereas Cl and Br do not and instead associate with a fluid phase; and (4) increasing temperature and CO_2 reduces partitioning of Cl into the fluid, along with other halogens.

Methods

Experimental and analytical rationale

The experimental and analytical approach used in this study differs in several ways from previous studies. Our starting materials are deliberately tailored to specific magmatic systems, with the exact compositions, including the observed crystal assemblage, and the partition experiments run at pressures and temperatures which matched their pre-eruptive (experimentally constrained) conditions (First et al. 2021; Cassidy et al. 2019). Capsules were not doped with added halogens. Only water ± carbon dioxide were added to reach fluid saturation. This approach was chosen to reproduce as close to "real" conditions as the magmas experienced at their respective pre-eruptive storage conditions (e.g., 50–100 MPa for the bulk basaltic andesite composition of Kelud and 120 MPa for the bulk dacitic composition of Quizapu equating to 2–5 km depth) and to ensure pressure, temperature, and $X_{H_2O}^{fluid}$, and brine-undersaturation conditions appropriate for the stored magmas (Cassidy et al. 2019; First et al. 2021). Due to the low concentrations and potential interferences, measurements were made by Secondary Ion Mass Spectrometry (SIMS). Despite the different experimental and analytical approaches, we find encouragingly similar partitioning values compared to previously published experiments using synthetic and doped natural starting materials (Online Materials[1] Table S1).

This study focuses on two active and well-characterized systems, which are typical of subduction zone magmas undergoing crustal storage and degassing, and span the intermediate-silicic compositional range that is involved in the enrichment of metals and for which halogen partitioning data are least abundant (Fig. 1; Online Materials[1] Table S1; Tattitch et al. 2021). Although some Cl data exist for compositions similar to Kelud and Quizapu (e.g., Zajacz et al. 2012), F and Br data are lacking, along with H_2O+CO_2-bearing experiments at low pressures that allow us to understand their fluid/melt partitioning.

Experimental procedure

Natural samples of crystal-bearing basaltic-andesite from Kelud volcano and dacite from Quizapu volcano (IGSN: PPRAI101F) were used as starting materials. The Kelud basaltic andesite contains 50–60% crystals of plagioclase, ortho- and clinopyroxene, magnetite, and matrix glass of dacite composition (Cassidy et al. 2016; Jeffery et al. 2013). The Quizapu dacite has a crystal content of 10–20 wt%, comprising plagioclase, amphibole, orthopyroxene, subordinate clinopyroxene, and accessory phases, including apatite, titanomagnetite, ilmenite, sulfide blebs, and zircon, together with a mostly rhyolitic matrix glass (Ruprecht et al. 2012). These samples were coarsely crushed (submillimeter size) to preserve the crystal cores. The cores act as nuclei, which become mantled by new crystal growth of a composition, which is in equilibrium with the evolved matrix melt in the experiments. This ensures a realistic composition of the "reactive melt" inside the shallow magmatic system (Pichavant et al. 2007; Erdmann et al. 2016). This approach was chosen as it more closely resembles natural conditions (i.e., melt, crystals, and bubbles) and minimizes concerns around structural changes to the melt and to the system overall, potentially affecting nucleation sites and crystallization kinetics, when starting from synthetic compounds or superliquidus conditions (Hammer 2008).

Approximately 0.1 g of sample was inserted into $Ag_{70}Pd_{30}$ capsules (wall thickness 0.25 mm, capsule diameter is 4 mm), together with ~0.01 g distilled water using a micro syringe, which was enough to saturate the melt in H_2O at the pressure and temperature of the experiments. The fluid to rock ratio was ~0.1 for most experiments; exact fluid masses were measured and used for subsequent mass balance calculations. For mixed volatile experiments, $AgCO_3$ powder was added in specific molar proportions along with specific quantities of water (measured by mass), to generate water fractions (X_{H_2O}) of 0.55 in the fluid phase [molar $X_{H_2O} = H_2O/(H_2O+CO_2)$]. X_{H_2O} of 0.55 was chosen to provide a contrasting but realistic value for comparison with pure water ($X_{H_2O} = 1$) experiments. Capsules were sealed closed using an arc welder.

Experiments below 900 °C were conducted in hydrothermal cold seal pressure vessels (using Rene 41 autoclaves) at the University of Oxford, United Kingdom. For experiments exceeding 900 °C, gas-pressurized cold seals, constructed of tungsten-zirconium-molybdenum (TZM) alloy with argon as the pressurizing medium, were used at the University of Mainz, Germany. To fix the oxygen fugacity for the gas pressured TZM experiments at the nickel-nickel-oxygen buffer (NNO), a double-capsule technique was used, whereby Ni powder was added to a platinum foil capsule and left open to equilibrate with the melt (Shea and Hammer 2013). In addition, methane was added as a reducing agent along with argon (0.4 MPa partial pressure), as tested in Shea and Hammer (2013). Ni metal powder (gray) oxidizes to green NiO, providing an easy visual check that the buffer is not exhausted at the end of the experiment. The oxidation conditions for the hydrothermal pressure vessels with Ni-Co alloy, Rene 41 autoclaves, were buffered at ~NNO by pure Nickel filler rods situated next to the capsule (Matthews et al. 2003).

A K-type thermocouple was inserted into a small hole in the end of the autoclave close to the capsule position to check for temperature offset between the furnace's internal thermocouple and autoclave. The samples were held at a constant pressure and temperature to replicate magmatic storage conditions for the specific volcanic systems, for up to 7 days (Table 1), and the experiments were then rapidly quenched (<1 min) in both cold seal and gas pressured experiments with a water-cooled system. Experimental run times were varied as a function of temperature, with a minimum of 25 h for experiments at 1100 °C for basaltic andesite runs and 160+ h for silicic compositions and temperature of 800–900 °C. These run durations are similar to other partitioning studies with the shortest durations that reached equilibrium in 3–4 h for chlorine partitioning experiments in basalts at 1200 °C (Alletti et al. 2009). However, Br diffusion is slower, which led Cadoux et al. (2018) to run their experiments at 1200 °C for 24 h, the minimum time used in our experiments. For silicic compositions, Kravchuk and Keppler (1994) ran partitioning experiments at 800 °C, varying run times between 93 and 1142 h with little difference to measured halogen contents. Capsules were weighed before and after welding and following quenching of the experiments to ensure no fluid loss occurred; if mass loss was recorded, the experiments were discarded. Backscattered electron imaging of the run products showed microlite-free glass (Online Materials[1] Fig. S1) with little chemical variability (Table 3).

Analytical techniques

Electron microprobe analysis (EMPA)

The starting materials and experimental glasses were made into polished resin mounts (Epo thin 2) and carbon coated. They were analyzed for their major element compositions by electron microprobe (EMPA) using a JEOL JXA 8200 superprobe at the University of Mainz and a Cameca SX-FiveFE at the University of Oxford. The operating conditions were: 15 kV accelerating voltage, 6–8 nA beam current, with a 10 µm defocused beam and counting times of 50–200 s per analysis. Na and K peaks were counted first and for short (15 s) duration to minimize

Table 1. Experiments conducted under NNO oxygen buffer

Experiment number	Starting material	*P* (MPa)	*T* (°C)	X_{H_2O} (wt%)	Glass content (vol%)	Volatile mass (g)	Glass mass (g)	Duration (h)
Kel14	Basaltic andesite	50	1000	1	43.9	0.0298	0.0162	49
Kel12	Basaltic andesite	50	1050	1	47.4	0.0044	0.0446	36
Kel9	Basaltic andesite	50	1100	1	39.5	0.0131	0.0409	24
Kel35	Basaltic andesite	50	1050	0.55	30.1	0.0144	0.0289	46
Kel34	Basaltic andesite	50	1025	1	36.9	0.0133	0.0433	42
Kel23	Basaltic andesite	50	1000	0.56	28.7	0.0302	0.0211	48
Kel2	Basaltic andesite	100	1000	1	31.0	0.0139	0.0212	44
Kel15	Basaltic andesite	100	1100	1	43.0	0.0056	0.0448	24
Quiz5	Dacite	120	900	1	92.1	0.0455	0.0852	168
Quiz4	Dacite	120	800	1	86.5	0.0076	0.0798	170
Quiz3	Dacite	120	850	1	94.6	0.0205	0.0844	171
Quiz16	Dacite	120	900	0.5	89.0	0.0019	0.0669	167
Quiz15	Dacite	120	800	0.56	82.4	0.0092	0.0596	178
Quiz13	Dacite	120	850	0.5	86.6	0.0220	0.0585	171

migration (Nielsen and Sigurdsson 1981). Chlorine and fluorine were measured on the PETH and TAP crystals, respectively, at counting times of 40 s each. A Phi-rho-Z correction for atomic number, absorption, and fluorescence was applied to all analyses, and the calibration was performed using a range of natural and synthetic reference materials. One σ standard deviations were generally <2% for most major elements analyzed. Secondary reference materials were measured on both EMPA instruments to ensure consistency and to assess the accuracy and precision, which can be found in Online Materials[1] Table S2.

Table 2. Starting conditions of matrix glass and XRF data, along with Br, Cl, and F contents

	Quizapu		Kelud	
	Matrix glass	Bulk rock	Matrix glass	Bulk rock
wt%	EMPA	XRF	EMPA	XRF
SiO_2	71.44	66.50	69.38	54.56
TiO_2	0.34	0.54	0.53	0.65
$Al2O_3$	14.85	15.74	15.42	18.86
FeO	1.59	2.97	4.00	8.89
MnO	0.07	0.09	0.15	0.21
MgO	0.33	0.87	1.04	3.73
CaO	1.13	2.38	3.54	9.13
Na_2O	4.39	5.13	4.26	2.79
K_2O	4.02	3.27	1.74	0.67
P_2O_5		0.14	0.20	0.12
Total	98.59	97.40	100.42	99.62
SIMS (ppm)	Sigma		Sigma	
F	661	44	564	56
Cl	2192	100	1476	14
Br	6.1	0.7	4.3	0.4

Note: Bulk-rock XRF from Ruprecht et al. (2012) (Quizapu) and Cassidy et al. (2019) (Kelud).

Scanning electron microscope (SEM) image analysis

Quantitative textural analysis of the glass was conducted using backscattered electron imagery combined with published energy-dispersive spectrometer (EDS) mapping from Cassidy et al. (2019). Carbon-coated samples were imaged at 15 kV, a working distance of ~10 mm, using a FEI Quanta 650 SEM at the University of Oxford. To measure the glass content of the initial starting powder and final experimental products >10 backscattered electron images of each sample were taken, and ~300 crystals were digitized using image processing software. The glass fraction was then quantified with ImageJ and is presented in Table 2.

Secondary ion mass spectrometry (SIMS) analysis

The polished resin mounts were gold-coated (~30 nm thickness) and analyzed on a Cameca IMS 1270 instrument at the NERC ion

Table 3. Major element and Br, Cl, and F contents of experiments, modelled water, and CO_2 values and fluid/melt partitioning [the standard deviation (1 sigma) of the multiple analyses for each experiment (n = 11–24)]

EMPA (wt%)	Kel14	Sigma	Kel12		Kel9		Kel35		Kel34		Kel23		Kel2		Kel15		Quiz5		Quiz4	
Cl	0.08	*0.01*	0.05	*0.01*	0.04	*0.04*	0.19	*0.10*	0.11	*0.03*	0.17	*0.03*	0.09	*0.01*	0.06	*0.02*				
SiO_2	67.57	1.24	58.41	0.86	56.64	0.93	71.70	1.87	68.83	0.91	71.59	1.53	67.21	0.82	59.70	1.23	67.95	0.49	68.71	1.03
TiO_2	0.60	0.06	0.91	0.11	0.67	0.06	0.79	0.16	0.69	0.14	0.69	0.08	0.51	0.14	0.75	0.09	0.29	0.01	0.24	0.11
Al_2O_3	14.08	0.25	14.64	0.56	16.01	0.36	11.87	0.22	13.98	0.70	12.88	0.62	14.15	0.20	13.97	0.27	14.43	0.23	13.99	0.86
FeO	2.81	0.49	9.31	0.99	7.75	0.57	6.31	1.25	2.98	0.17	2.80	0.39	2.10	0.26	5.86	0.46	1.35	0.05	1.02	0.29
MnO	0.13	0.02	0.24	0.04	0.22	0.04	0.18	0.04	0.13	0.03	0.12	0.03	0.13	0.03	0.23	0.03	0.06	*0.02*	0.05	*0.03*
MgO	1.17	0.23	3.29	0.26	3.90	0.65	0.91	0.13	1.27	0.14	0.88	0.59	1.26	0.14	3.52	0.31	0.27	*0.01*	0.48	*0.54*
CaO	3.17	0.32	6.95	0.21	7.88	0.68	3.13	0.53	2.72	0.62	1.97	0.30	2.87	0.21	6.44	0.49	1.14	*0.03*	0.97	*0.34*
Na_2O	4.94	0.15	3.44	0.21	3.28	0.18	4.22	0.14	5.01	0.20	5.06	0.33	4.24	0.09	3.94	0.15	3.25	0.31	3.26	0.59
K_2O	1.77	0.12	1.03	0.07	0.80	0.09	1.67	0.27	1.72	0.19	2.08	0.11	1.61	0.09	1.13	0.10	3.56	0.13	3.70	0.33
P_2O_5	0.22	0.02	0.18	0.03	0.17	0.02	0.31	0.09	0.30	0.04	0.27	0.04	0.20	0.02	0.19	0.04	0.04	0.02	0.04	0.04
Total	96.62	0.25	98.53	0.40	97.40	0.67	101.34	0.73	97.82	0.44	98.56	0.77	94.44	0.32	95.83	0.45	92.34	0.98	92.46	1.10
Modeled dissolved volatiles (wt%)																				
H_2O	2.48		2.69		2.47		1.72		2.53		1.59		3.68		3.79		4.35		4.35	
CO_2	0		0		0		0.02		0		0.02		0		0		0		0	
SIMS (ppm)																				
F	451	*17*	342	*33*	231	*24*	497	108	528	18	500	94	555	22	496	5	527	9	706	60
DF fl/melt	0.96	0.15	4.46	2.09	4.91	1.41	1.16	0.95	0.66	0.09	0.45	0.29	0.54	0.05	0.71	0.03	0.28	0.08	0.03	0.03
Cl	1373	*88*	659	*86*	530	*116*	1507	220	1652	104	2110	409	969	35	700	4	486	5	966	84
DCl fl/melt	0.75	0.04	9.66	2.12	6.05	2.30	0.73	0.16	0.02	0.02	0.02	0.02	1.56	0.10	8.18	0.70	5.85	0.33	12.69	2.78
Br	2.2	*0.9*	1.3	*0.3*	1.1	*0.3*	2.8	0.8	2.0	0.0	1.5	0.3	2.3	0.4	1.6	0.2	1.0	0.0	1.3	0.1
DBr fl/melt	1.85	0.80	20.26	10.82	10.38	5.87	2.33	2.01	4.88	0.28	2.19	0.96	2.25	0.97	13.07	3.74	8.95	1.70	36.40	8.30

(Table extends on next page.)

microprobe facility at the University of Edinburgh. The samples were placed in a vacuum to outgas for >14 h prior to analyses. Vacuum in the main chamber during analysis was $<5 \times 10^{-8}$ Torr.

Halogen analyses were performed in two different sessions, both using a 10 kV, Cs+ primary ion beam of ~2 nA for Cl and F, and ~7 nA for Br, with the normal incidence electron flood gun for charge neutralization and the electron multiplier (EM0) as the secondary ion detector. After pre-sputtering for 60 s, the magnet calibration was checked and the automated secondary beam alignment was adjusted using either ^{18}O or $^{30}Si^{16}O_3$ as the reference peak.

For F and Cl analysis ^{18}O, ^{19}F, ^{30}Si, and ^{35}Cl were measured at a mass resolution of 3200, an energy window of 60 eV, an analyzed region of ~7 × 10 µm and magnetic peak switching. Each analysis consisted of 10 cycles, in which ^{28}Si and ^{18}O were counted for 2 s each and ^{19}F and ^{35}Cl for 4 s each. The secondary ion beam intensity measured at masses ^{19}F and ^{35}Cl were normalized to ^{18}O. To calculate the sample composition, we used MPI-DING reference glasses (StHs80, ML-3BG, T1G, ATHO-G; Jochum et al. 2006) and the USGS reference glass BCR-2G. The fluorine concentration of the unknown sample was given by:

$$F_{concentration} = \left[\frac{^{19}F(cps)}{^{18}O(cps)}\right] * Relative\ Ion\ Yield$$

where the cps refers to counts per second, Relative Ion Yield = (Ion Yield F/Ion Yield O) averaged over multiple primary standards, and

Ion Yield F = ^{19}F(cps)/known F concentration, and
Ion Yield O = ^{18}O(cps)/known O concentration.

Chlorine concentrations were given by similar equations for the ^{35}Cl count rate (cps) normalized to the ^{18}O count rate (cps).

The standard deviation of the primary standard calibration of the Relative Ion Yields for F and Cl were lower than 4%.

For Br analysis, a mass resolution of 21 000 was used with a 2000 µm field aperture giving an analyzed region of ~7 × 10 µm. Each analysis consisted of 10 measurement cycles, with $^{30}Si^{16}O_3$ being measured for 2 s each cycle and ^{79}Br and ^{81}Br measured for 5 s each cycle. For Br, we used GSC-1G, GSE-1G, GSD-1G, BB1, and BB2 (Online Materials[1] Fig. S2) as our standard reference materials (Marks et al. 2017; Kendrick 2012). The halogen concentrations of the unknown glasses were then calculated as follows:

$$Br_{concentrations} = \frac{^{81}Br(cps) + ^{79}Br(cps)}{\left[^{30}SiO^{16}O_3 \frac{cps}{Si_{conc}(known)}\right]} * Relative\ Ion\ Yield$$

where the Relative Ion Yield is given by = (Ion Yield of Br/Ion Yield Si) for an average of multiple primary standards (Online Materials[1] Table S2; Online Materials[1] Fig. S3) mounted in each sample block, and

Ion Yield Br = [$^{79}Br(cps) + ^{81}Br(cps)$] / known Br concentration (primary standard), and
Ion Yield Si = $^{30}Si^{16}O_3$ (cps) / known Si concentration (primary standard).

The Si content of the experiments was sometimes higher than the standards for Br (Online Materials[1] Table S2); however, as Br ionizes well, as shown by relatively stable signal intensities, matrix glass effects are considered here to be minimal. This is supported by the secondary standard comparison plot (Online Materials[1] Fig. S2) for the five secondary standards, each with a different major element composition, showing a good match between measured and accepted values. Typically, seven analyses were measured per sample. Mean concentrations and standard deviations are given in Table 3, and show good reproducibility. Along with the unknown samples, MPI-DING secondary reference glasses were measured throughout the analysis session to check for reproducibility, accuracy and drift (Online Materials[1] Table S2). Limits of detection (estimated based on the number of counts per time counted, see Online Materials[1] Table S2) for Cl and F were calculated on reference glasses StHs80 for F and Cl, and scapolite BB1 and GSE-1G for Br, equating to 0.5, 1.3, and 0.35 ppm for F, Cl, and Br, respectively.

We found that the halogen concentrations for the secondary reference materials varied slightly between different mounts, potentially affected by the sample height, suggesting that calibration should be conducted on the same mounts as the sample analysis if possible.

TABLE 3.—*EXTENDED*

EMPA (wt%)	Quiz3		Quiz16		Quiz15		Quiz13	
Cl			0.29	0.01	0.06	0.01	0.11	0.02
SiO_2	66.43	0.51	69.71	0.34	68.74	1.05	68.63	0.58
TiO_2	0.32	0.02	0.35	0.02	0.26	0.11	0.30	0.02
Al_2O_3	15.46	0.27	14.64	0.13	15.00	1.47	14.61	0.19
FeO	1.78	0.11	1.54	0.10	1.12	0.27	1.20	0.09
MnO	0.09	*0.02*	0.07	*0.02*	0.06	*0.02*	0.06	*0.03*
MgO	0.47	*0.03*	0.35	0.02	0.18	0.18	0.26	0.02
CaO	1.67	*0.07*	1.03	*0.03*	1.19	*0.56*	1.05	*0.06*
Na_2O	3.82	0.11	4.47	*0.14*	4.35	*0.57*	3.93	*0.21*
K_2O	3.43	0.07	3.98	0.06	3.76	0.45	3.85	0.07
P_2O_5	0.05	0.03						
Total	93.51	0.31	96.45	0.43	94.74	1.44	94.01	0.84
Modeled dissolved volatiles (wt%)								
H_2O	4.36		2.24		2.92		2.36	
CO_2	0		0.05		0.03		0.05	
SIMS (ppm)								
F	345	11	643	6	461	5	490	12
DF fl/melt		3.41	0.24	0.24	3.14	0.36	0.90	0.18
Cl	257	27	1578	49	652	3	495	4
DCl fl/melt			11.87	1.74	16.07	0.76	9.04	0.49
Br	0.4	0.1	3.5	0.2	0.5	0.4	0.8	0.0
DBr fl/melt		70.59	23.26	9.09	69.24	36.72	18.84	2.93

RESULTS

Petrological description of run products

The run products range in glass contents from 28–47 wt% for Kelud and 82–94 wt% in the Quizapu experiments (Table 1). No new phases relative to the starting materials appeared during the experiments; however, in some of the lower-temperature experiments, more-evolved rims can be observed in backscattered images, compared to some more primitive crystal cores (Online Materials[1] Fig. S1). This suggests that mineral rims grew in equilibrium with the melt as intended by experimental design, without reacting with the more primitive mineral cores (Pichavant et al. 2007). The experimental glass was microlite poor (Online Materials[1] Fig. S1) and contained vapor vesicles,

indicative of fluid saturation, which was confirmed by puncturing and heating the capsule post-experiment and determining relative mass loss. Repeat analyses of major element and halogen concentrations (n = 7–24) of experimental glass showed them to be homogenous (Fig. 2) within analytical uncertainty (Online Materials[1] Table S3), suggesting that the time chosen to reach chemical equilibrium was appropriate (Table 1).

Halogen concentrations in matrix glass

Although Cl measured both by electron microprobe (EMPA) and SIMS (Online Materials[1] Fig. S4) were correlated, the concentrations of Cl were close to or below the limit of detection for EMPA, as the instrument setup was not optimized for Cl measurements. We therefore report SIMS results in this paper, with their precision values <12%, and accuracy (<20% for Br and <2% for Cl and F values >100 ppm) supported by analysis of secondary reference glasses (Online Materials[1] Table S2).

The mean values, measured by SIMS, for the Kelud matrix glass composition (dacite) were: F = 564 ppm (±56; 1 standard deviation of reproducibility), Cl = 1476 ppm (±14), and Br = 4.3 ppm (±0.4). For the Quizapu matrix glass composition (rhyolite): F = 661 ppm (±44), Cl = 2192 ppm (±100), and Br = 6.1 ppm (±0.75) (Table 2). Note that two bromine measurements of 0.42 ppm (Quiz 3) and 0.54 ppm (Quiz 5) are close to the detection limit of bromine of 0.35 ppm. Minor quantities of hydrous minerals (<1% of halogen-bearing apatite and <2% amphibole in the Quizapu experiments) may slightly alter the absolute halogen contents in bulk starting material experiments.

Experimental matrix glass compositions range from andesitic to rhyolitic for Kelud (Table 1; Fig. 2), with the Quizapu experiments limited to rhyolitic glass compositions (Table 3). The range of compositions exhibited in the experimental glasses can be attributed to varying amounts of melting and crystallization resulting from the varying experimental run temperatures, fluid contents, and compositions (X_{H_2O}). Thus, variable crystallinity may dilute or enrich the halogen content in the glass for different experiments (Table 1). Figure 2 shows SiO_2 vs. Cl, F, and Br glass concentrations for all experiments. For the Kelud starting composition (Table 2), the experimental products with more evolved compositions contain higher F, Cl, and Br concentrations in the natural matrix glass. These positive correlations with SiO_2 for fluorine ($R^2 = 0.68$), chlorine ($R^2 = 0.73$), and bromine ($R^2 = 0.55$) exist despite changes in experimental pressure, temperature, and volatile composition. For the Quizapu starting composition (Table 2), this trend of increasing halogen concentrations at higher SiO_2 concentrations is apparent, despite the more limited range in compositions in the experimental matrix glass, e.g., for fluorine $R^2 = 0.54$. For chlorine and bromine, the correlation only exists for the water-saturated experiments ($X_{H_2O} = 1$), with correlation coefficients R^2 of 0.76 and 0.96 for Cl and Br, respectively. The mixed volatile experiments from Quizapu (green open symbols, Fig. 2) mostly fall within the same range as the water-saturated experiments.

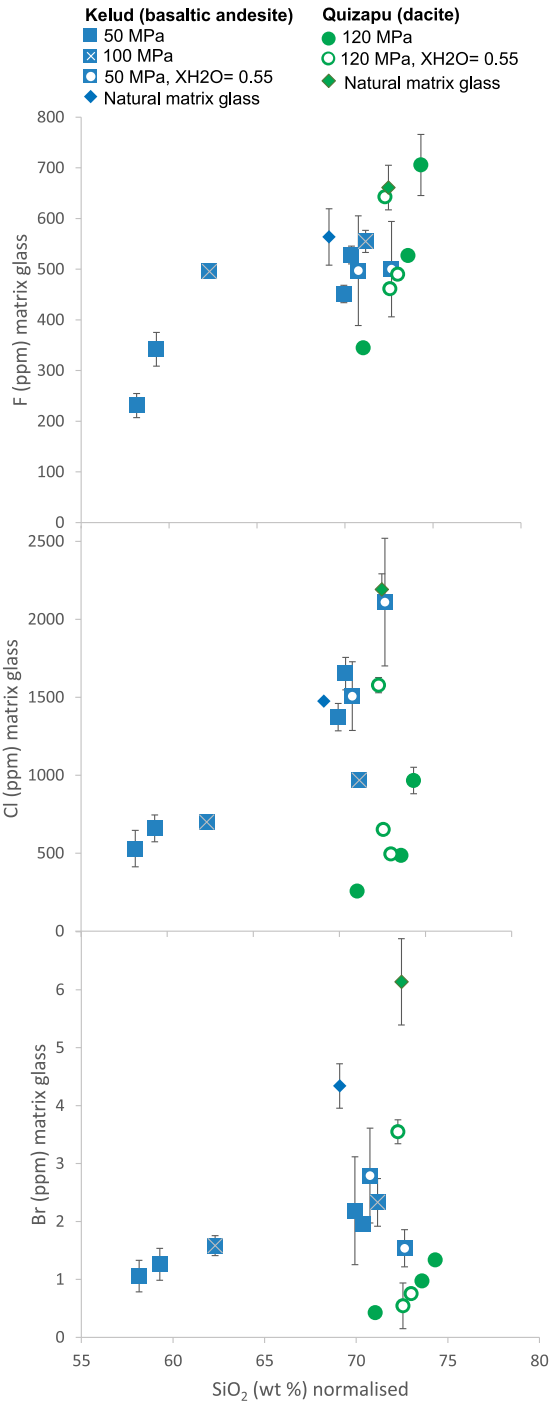

Figure 2. SiO_2 vs. halogen concentrations in experimental glass products, along with their natural matrix glass compositions. Errors given are 1 standard deviation of the range of the values measured. (Color online.)

Halogen fluid composition

To work out the fluid composition required for calculating the fluid/melt partitioning, we used a simple mass balance approach similar to Cadoux et al. (2018):

Mass (g) of halogen in fluid = Mass of halogen in starting glass – Mass of halogen in final glass

whereby,

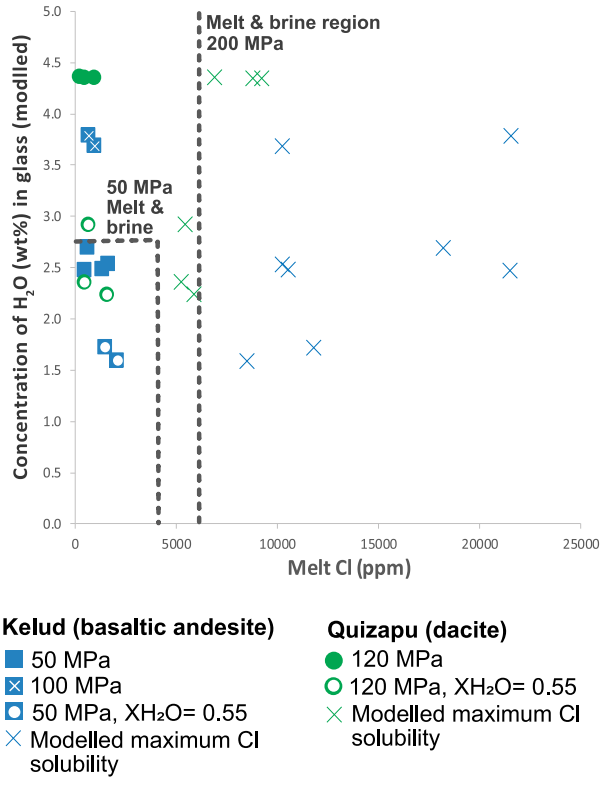

Figure 3. Showing Cl melt contents of the experiments of Quizapu, dacite starting material (green) and Kelud, basaltic andesite starting material (blue), with the corresponding modeled H_2O contents from MELTS. The dashed lines indicate where brine and vapor phases appear at 50 and 200 MPa pressures. The crosses indicate the maximum Cl contents for each experiment as modeled using Webster et al. (2015) Cl solubility model. Our experiments show brine-undersaturated conditions. (Color online.)

Mass of halogen in starting powder = Concentration of halogen in starting powder (ppm) * 10^{-6} × Mass of starting powder (g).

The measured masses were converted into mass of glass, by correcting for the crystal fraction in the starting material and the final glass as measured with SEM image analysis (Table 1).

Mass (g) of halogen in the final glass = Concentration of halogen in final glass (ppm) × 10^{-6} × Corrected mass of final glass (g)

The corrected mass of the final glass is calculated from the initial mass of glass combined with the mass of volatiles added to the capsule that dissolved within the melt. This correction involves the respective gain and/or loss of water and CO_2, which partitioned from the volatile phase in favor of the melt phase during the course of the experiment. These volatile contents were modeled using a MELTS H_2O and CO_2 solubility model, requiring the pressure, temperature, X_{H_2O}, and melt composition (Gualda and Ghiorso 2015). The modeled volatile contents are comparable to other models (e.g., Papale et al. 2006).

Fluid concentration of halogen (ppm) =
Mass (g) of halogen in fluid / corrected final fluid mass (g) × 10^6

The uncorrected fluid mass was the measured weight of added volatiles to the capsule. The mass difference between the final and initial glass was subtracted to give the corrected fluid mass. At equilibrium during high-*P*-*T* experiments there is a subtle impact of partial dissolution of the aluminosilicate melt into the coexisting volatile phase (Burnham 1967). At the relatively low pressures of these experiments, Burnham (1967) showed that only a small amount of solute dissolved into the coexisting fluid (<2 wt%). A 2% correction was made to the masses of the initial powder and volatile phase for all experiments. The partition coefficient for each halogen was calculated by dividing the halogen concentration of the fluid by that of the melt.

Uncertainties were propagated using the minimum and maximum halogen concentrations in the initial and experimental glasses, adjusting for crystal content calculation errors (±5 wt%), weighing errors and calculated masses of H_2O and CO_2 (Table 3). The propagated errors are plotted in Figures 3 to 8. Previous studies have shown that these propagated errors often overestimate the absolute error and thus can be considered maximum values (e.g., Alletti et al. 2014; Cadoux et al. 2018). Finally, Quizapu and Kelud both contain trace amounts of apatite (<1 vol%) and Quizapu contains ~2 vol% hornblende (Hildreth and Drake 1992; Ruprecht et al. 2012; Ruprecht and Bachmann 2010; Jeffery et al. 2013; Cassidy et al. 2016, 2019; First et al. 2021). Hydrous minerals may incorporate halogens into the mineral structure, but the low abundance of hydrous minerals, coupled with knowledge of mineral/melt partitioning values (e.g., Doherty et al. 2014; Iveson et al. 2017; Marks et al. 2012) suggests that minor amounts of crystallization or melting of apatite and/or hornblende during the experiment would have a minimal effect on our $D^{fluid/melt}$ values. Given typical F and Cl contents in hornblende for Quizapu and arc magmas, this constitutes <10 ppm of Cl and <50 ppm of F being added to the melt if hornblende is completely dissolved.

Fluid/melt halogen partitioning

No additional halogen sources were added to the starting materials and, given that measured melt Cl contents are an order of magnitude below the modeled maximum Cl solubilities (Fig. 3) (Webster et al. 2015), none of these experiments reached hydrosaline brine saturation, despite the addition of CO_2 in some experiments, which can lower the threshold for brine-saturation (Joyce and Holloway 1993). The run product glasses lie within the experimentally constrained "200 MPa melt + aqueous vapor field" for rhyolitic melts in equilibrium with a low-density volatile phase (Webster et al. 2015; Fig. 3).

For all experiments, the halogen fluid concentrations show broad positive correlations with bulk fluid/melt partition coefficients consistent with other studies and largely independent of temperature, pressure, and volatile contents (Figs. 4 and 5). Fluid concentration uncertainties were slightly higher for F and Br mass balance calculations, and these graphs show more scatter than for Cl, which is a function of the larger range measured in glass halogen contents for these experiments. The mixed volatile experiments (X_{H_2O} = 0.55) fall on the generally positive trend, as do the higher pressure (100 MPa) Kelud experiments.

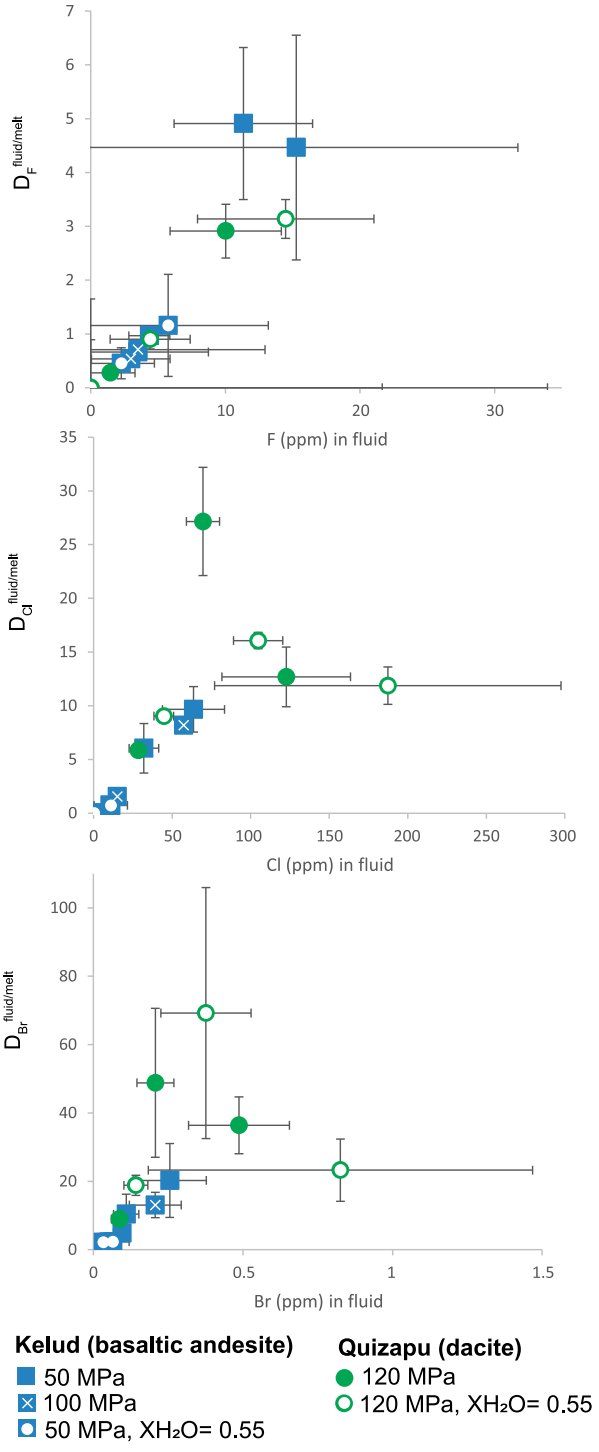

Figure 4. Mass balance calculated fluid halogen concentrations, against halogen fluid-melt partitioning. Maximum accumulated errors are plotted. (Color online.)

A clear outlier to the generally positive correlations is Quiz 3 (850 °C, X_{H_2O} = 1; Table 3), which yields higher than expected fluid/melt partitioning values relative to its fluid concentration (e.g., Fig. 4). This can be attributed to a higher actual fluid mass than calculated, which is corroborated by the prominent H_2O resorption haloes around the bubbles in the SEM images for Quiz 3 (Online Materials[1] Fig. S1). Consequently, this point was removed from the following data set presented.

Partitioning and ionic radius

Bureau et al. (2000) suggested that $D^{fluid/melt}$ increases with ionic radius for halogens in albite melt, although Cadoux et al. (2018) suggested further complexity to this relationship depending on melt composition and volatile content and based on deductions from gas geochemistry. The new experiments presented here are consistent with $D^{fluid/melt}$ increasing with ionic radius (Fig. 5), though with higher $D_F^{fluid/melt}$ values than Bureau et al. (2000). On average, $D^{fluid/melt}$ for F [smallest ionic radius, D = 1.4 ± 0.51 (mean absolute error)] is lower than Cl (D = 6.4 ± 0.9), which is in turn lower than Br (largest ionic radius; D = 16.5 ± 6.5). These values are within the range measured for halogens in other studies on similar melt compositions (Online Materials[1] Table S1). The average data can be fitted using an exponential function with a R^2 of 0.95, but the best-fitted data are the Quizapu data set shown in green (Fig. 5; R^2 = 0.99). The less-evolved Kelud experiments have a lower average bulk $D^{fluid/melt}$ than the more evolved Quizapu experiments for chlorine and bromine, but yield higher values for fluorine. This observation may not be significant given the range of partitioning values; however, it is consistent with the

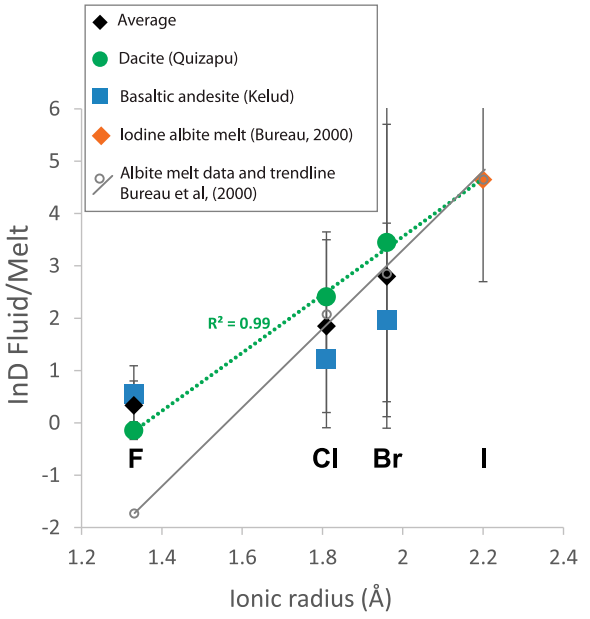

Figure 5. Plot of natural log of fluid/melt F, Cl, and Br partitioning values in this study and iodine value from Bureau (2000) against ionic radius in angstroms. For comparison the data set and trendline from Bureau et al. (2000) is plotted. The green trendline shown is from the Quizapu data set, which represents the best correlation. Error bars indicate 1 standard deviation of the values for the pressures (50–120 MPa), temperatures (800–1100 °C) and X_{H_2O} (0.55–1) conditions. The biggest difference is the differing F partitioning values (higher in this study) which alters the regression equation. The F partitioning value in Bureau et al. (2000), was from Webster et al. (1992), measured in granitic melts. (Color online.)

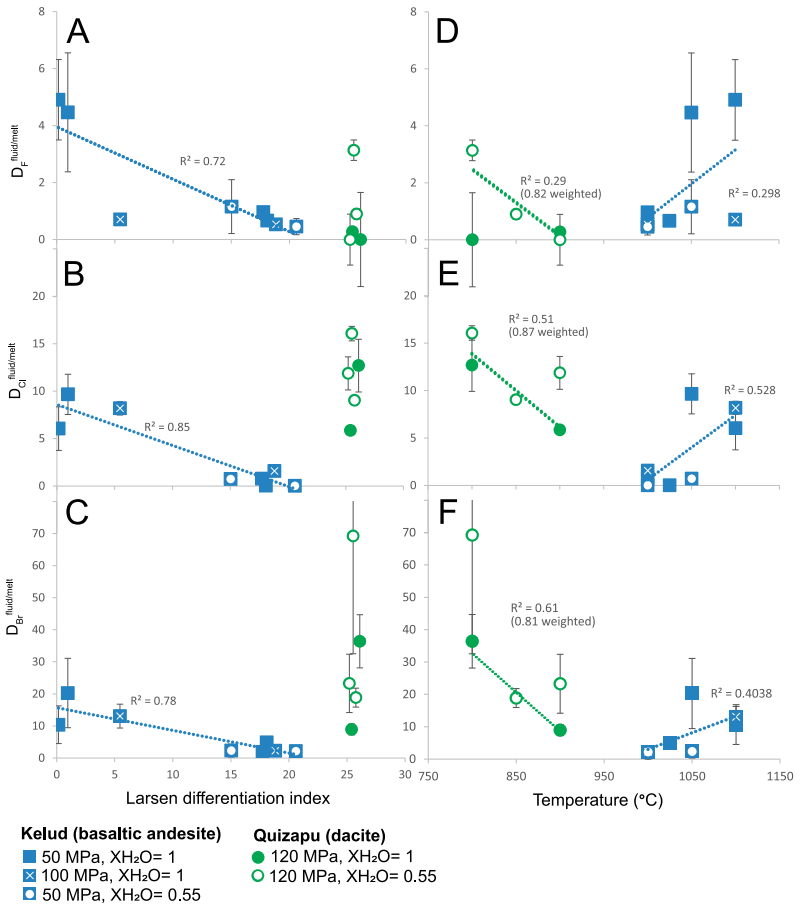

Figure 6. Effects of glass composition (Larsen differentiation) and temperature on bulk partitioning of halogens. R^2 values shown above report both the unweighted and weighted regressions. Variance-weighted regression was applied to Quizapu data set, which has higher uncertainties (**d**, **e**, and **f**), providing revised R^2 values and the trend lines against temperature plotted above. (Color online.)

more evolved granitic melt value (76 wt% SiO_2 from Webster (1990) for $D_F^{fluid/melt}$, which is even lower.

Halogen fluid/melt partitioning as a function of changing intrinsic variables

To assess the effects of varying melt composition on halogen $D^{fluid/melt}$, we plot our experimental data against the Larsen differentiation index $(0.33\times SiO_2+K_2O)-(FeO+MgO+CaO)$ (Larsen 1938) (Figs. 6a–6c). This has been shown to be a useful index for characterizing evolving melt composition especially for Cl (e.g., Webster et al. 2020). It accounts for elements known to control Cl solubility (e.g., Ca, Mg, and Fe; Webster et al. 2015) without using Na, which is prone to electron-beam migration in hydrous glasses. The Quizapu data show a very limited compositional change, yet a range in $D^{fluid/melt}$ (Figs. 6a–6c). In contrast, the Kelud experimental glasses exhibit a wide range in glass compositions (andesite to rhyolite) and form shallow negative trends with respect to $D^{fluid/melt}$ with R^2 all above 0.72, with Cl particularly well correlated. In the case of fluorine, this trend extends toward the more evolved Quizapu compositions (R^2 = 0.5) (Fig. 6a). However, there is no significant trend with differentiation for Br and Cl when Kelud and Quizapu data sets are combined. The melt differentiation trends in the Kelud data set occur despite superimposed differences in pressures, CO_2-H_2O mixtures, temperatures, and potential errors relating to the fluid calculation.

Kelud and Quizapu experiments show opposite trends as a function of temperature (Fig. 6d–6f). While $D^{fluid/melt}$ in the Quizapu dacite series decreases with higher temperature, $D^{fluid/melt}$ in Kelud increases with temperature. The temperature effect on $D^{fluid/melt}$ values is most pronounced for the Quizapu data set and for Br (R^2 = 0.61), with F less temperature-dependent. Due to the large uncertainties of some Quizapu experiments, variance-weighted regression was applied to temperature correlation, providing higher revised R^2 correlations of 0.82, 0.87, and 0.81, for F, Cl, and Br, respectively.

All experiments were fluid saturated, but mixed volatile experiments with varying CO_2 and H_2O ratios were run to assess their effect on fluid/melt partitioning of halogens (Fig. 6). In both the Kelud and Quizapu data set, the CO_2 bearing experiments (X_{H_2O} = 0.55) lie along the same trends as the X_{H_2O} = 1 series; however, the CO_2-bearing experiments generally show lower $D^{fluid/melt}$ values (Fig. 6). For the Kelud experiments, mean fluid/melt partition coefficients for the X_{H_2O} = 1 experiments are F = 2 ± 1.9 (1 s.d.), Cl = 4.4 ± 3.8, and Br = 8.8 ± 6.6 (n = 6). For the X_{H_2O} = 0.55 experiments these are F = 0.8 ± 0.3, Cl = 0.4 ± 0.4, and Br = 2.3 ± 0.1 (n = 2). For Quizapu, the X_{H_2O} = 1 experiments had mean fluid/melt ratios of F = 0.1 ± 0.1, Cl = 9.3 ± 3.4, and Br = 22.7 ± 13.7 (n = 2); while the X_{H_2O} = 0.55 experiments had $D^{fluid/melt}$ values; F = 1.4 ± 1.3, Cl = 12.3 ± 2.9, and Br = 37.1 ± 22.8, showing higher $D^{fluid/melt}$ values.

Figure 7 highlights in detail how $D^{fluid/melt}$ covaries with various elements for the combined Kelud and Quizapu experimental data set. Pearson correlation values suggest that $D_{Cl}^{fluid/melt}$ and $D_{Br}^{fluid/melt}$ generally behave in a similar way (correlation coefficient = 0.88), with highest negative correlations for Ti (also Na in the case for Cl) and positive correlations Al and K. While $D_F^{fluid/melt}$ behaves markedly differently from $D_{Cl}^{fluid/melt}$ and $D_{Br}^{fluid/melt}$ (coefficient = 0.24 and 0.26) and negatively correlates best with Si, Na, and K, with positive correlations for Fe, Mg, and Ca. The differences between the Kelud and Quizapu data sets can be seen in Online Materials[1] Figures S5 and S6.

Halogen fluid/melt partitioning across different studies

Values for $D_{Cl}^{fluid/melt}$ are all <20 (Figs. 6b and 6e), in line with other studies at similar melt compositions and experimental

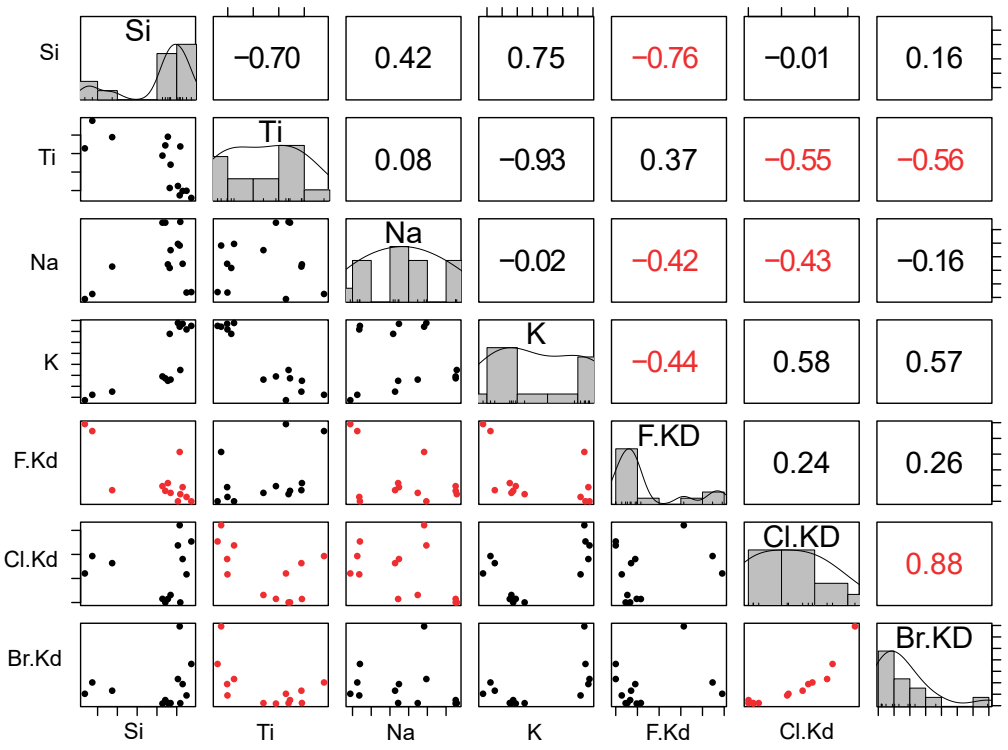

FIGURE 7. Scatter plot of matrices of different elements and the Cl, F, and Br partitioning values, with bivariate scatter plots below the diagonal, histograms on the diagonal, and the Pearson correlation above the diagonal. The key correlations are highlighted in red. In the scatter plots the X axes represent the range of values of the element in the same row, while the Y axes represent the element in the vertical column. (Color online.)

conditions (e.g., Baker and Alletti 2012; Webster et al. 1999; Zajacz et al. 2012) (Online Materials[1] Table S1). The majority of experiments show that Cl predominantly partitions into the fluid phase over the melt phase, with the exception of two Kelud experiments ($D_{Cl}^{fluid/melt} < 1$). Relative to Cl, absolute $D_{F}^{fluid/melt}$ values are lower (<6) with a cluster around 1 for the most differentiated melts. Values for Br partitioning are the highest among the halogens measured in this study, a trend observed by Bureau et al. (2000), with most partition coefficients ranging between 2 and 36 (Online Materials[1] Table S1). In contrast to Cl and F, which partition into the melt under some conditions, our Br data show that it strongly partitions into the fluid phase in all the experiments.

Figure 8 plots our experiments in the context of other data from the literature (see Online Materials[1] Fig. S7 for full breakdown of the different studies). We use the aluminosity index A/CNK [molar Al/(Ca + Na + K)], as Cl and F melt solubility are affected by increasing network-modifying Na, K, and Ca relative to Al (Fig. 7) (Webster 1992; Signorelli and Carroll 2000; Webster et al. 2015). The literature data plotted are from experiments thought to be in the brine-undersaturated region for Cl, F, and therefore thought to represent Henrian partitioning. This was estimated using the region of parameter space defined in previous studies (e.g., Cl < 0.25 wt%, and F < 4 wt%; cf. Baker and Alletti 2012; Dolejš and Zajacz 2018; Shinohara 2009; Webster et al. 2015; Zajacz et al. 2012). However, some CO_2-bearing experiments from the literature may be in the brine field, as the presence of CO_2 lowers the threshold for brine saturation (e.g., Joyce and Holloway 1993). Figure 8 broadly highlights that the fluid/melt partition coefficients found in this study overlap with literature experiments at similar values on the aluminosity index. The Quizapu data set for instance, has similar values to those of Alletti et al. (2009) and Botcharnikov et al. (2015), yet higher than others (Zajacz et al. 2012). Kelud's experimental glass composition also overlapped with other studies (Hsu et al. 2019; Webster et al. 2017; Webster and Holloway 1990) and provides similar partitioning values. The literature data for CO_2 mixed volatile experiments in Figure 8 are plotted as open circles, and these generally occupy lower fluid/melt ratios for Cl (mean = 9.2), compared to water-saturated experiments (mean = 15); however, their relative standard deviations both exceed 100%. For CO_2-bearing F partitioning experiments, there is only this study and a few data points from Webster et al. (2014) to compare (Fig. 8b), nevertheless, the presence of CO_2 did not significantly influence $D_{F}^{fluid/melt}$. The only Br mixed volatile data are from this study and do not show significant differences with water-saturated experiments. Apart from the mixed volatile experiments, the data compilation in Figure 8 broadly shows that lower A/CNK values are associated with lower Br fluid/melt ratios (see also Online Materials[1] Table S1). For F, however, the opposite is true, with higher $D_{F}^{fluid/melt}$ values at the lower A/CNK values. There is no clear trend for $D_{Cl}^{fluid/melt}$, which speaks to the range of experimental conditions

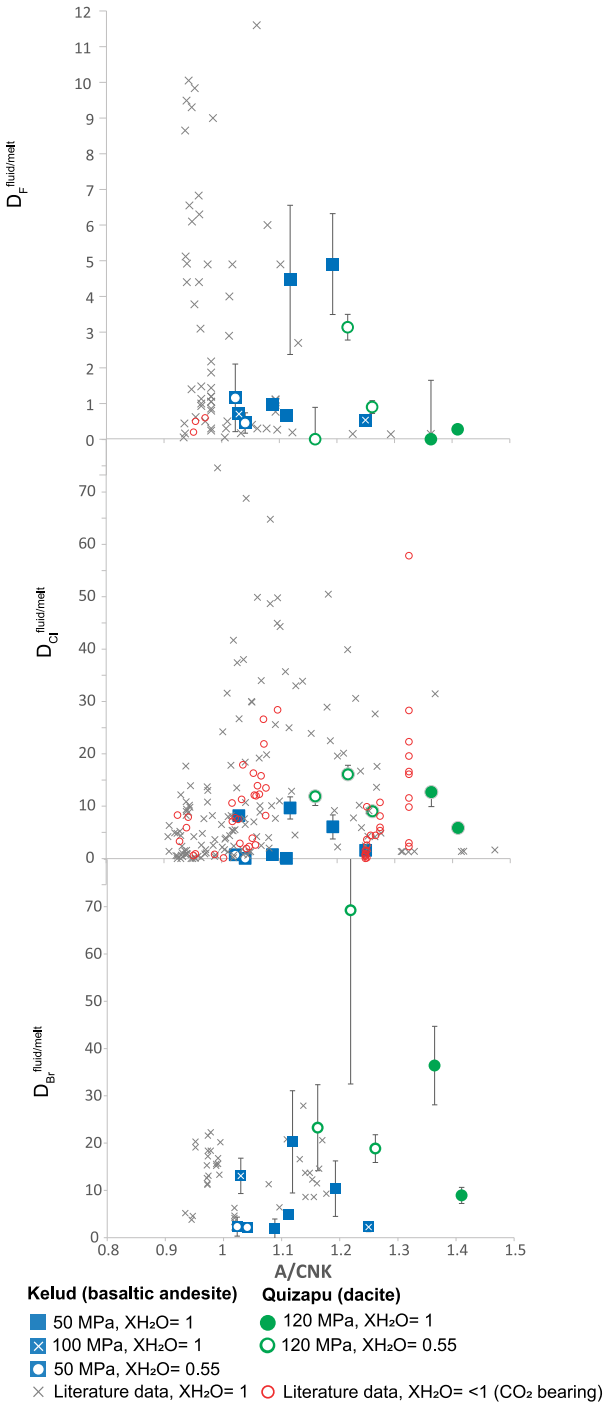

Figure 8. The molar A/CNK ratio for data in these study as a comparison to data from literature (including CO_2-bearing systems) for non-brine systems, and therefore thought to represent Henrian partitioning. Literature sources in Online Materials[1] Table S1 and broken down by study in Online Materials[1] Figure S7. (Color online.)

and the complexity of these data as well as the clustering of experiments in certain areas of A/CNK space (e.g., a sparsity of experiments at higher values).

Discussion

Halogen partitioning and its influences

The concentration of Cl in the fluid phase has been established as one of the primary controls on fluid melt partitioning (e.g., Webster 1992), which is confirmed by this study for Cl and also for F and Br (Fig. 4). The scatter in the data, i.e., for a constant halogen fluid concentration, may be explained by the differing melt compositions and conditions (Dolejš and Zajacz 2018). The sections below will cover how our experimentally derived halogen partitioning data are influenced by key variables such as ionic radius, melt composition, X_{H_2O}, and temperature, in the context of previous studies. While much of this has been studied for Cl, there is complexity (e.g., Fig. 8), and fewer data points exist for F and Br (Fig. 1).

Effect of ionic radius

Bureau et al. (2000) observed that for an albite melt composition, increasing fluid/melt partitioning values from F, Cl, Br, to I correlate with increasing ionic radii of the anion (Fig. 5). This relationship has also been shown for the fluid/melt partitioning behavior of the alkali metals Li, K, and Rb (e.g., Iveson et al. 2019). This result agrees with previous studies, which dictate that for the larger anions (Cl and Br), there is a greater mismatch with the ionic radius of O, making them less likely to be incorporated in the aluminosilicate network (Bureau et al. 2000). The iodine partitioning data of Bureau et al. (2000) (Fig. 5), can be used to extend the partitioning–ionic radius correlation from our Quizapu (rhyolite glass) experiments ($R^2 = 0.99$), which is more similar in composition to Bureau et al. (2000) than the Kelud data set. We use this correlation to form a revised weighted regression equation for rhyolitic melts based on our experiments as a function of ionic radius:

$$D_{\text{Halogen}}^{\text{fluid/melt}} = e^{[5.46(\pm0.09)\times Å - 7.41(\pm0.12)]},$$

where Å is the ionic radius in angstroms.

The gradient of the slope (and thus the preceding equation), will vary as a result of the chemical composition, for instance, mafic melts with higher $D_F^{\text{fluid/melt}}$ (Figs. 6 and 8) will lead to shallower gradients and vice versa (e.g., Bureau et al. 2000). The large variability in these values means that the highest $D_F^{\text{fluid/melt}}$ values are sometimes higher than the lowest $D_{Br}^{\text{fluid/melt}}$ values (Fig. 5), suggesting that other factors such as differences in halogen fluid concentrations, melt compositions, pressure, temperature, and X_{H_2O} may account for the variability in this trend.

Effect of melt composition

The two different starting compositions used in this study (whole rock basaltic andesite and dacite, with dacitic and rhyolitic initial matrix glass compositions, respectively) and variable *P-T* conditions produced a range of different melt compositions, which allows us to explore the role of composition on fluid/melt partitioning. Taking both data sets together, the highest $D_{Cl}^{\text{fluid/melt}}$ and $D_{Br}^{\text{fluid/melt}}$ values are found in the most differentiated melts (Fig. 6), yet the least differentiated melts did not necessarily show the lowest fluid/melt partitioning. In contrast, $D_F^{\text{fluid/melt}}$ shows the opposite trend across both data sets, with increasing

differentiation leading to lower average $D_F^{fluid/melt}$ values (Fig. 6).

The notion of increased Cl in the fluid phase at more-evolved compositions has been observed in multiple studies (e.g., Webster and De Vivo 2002) and also for Br (Cadoux et al. 2018). This is likely related to the incompatible nature of the larger ions, Cl and Br in melts during differentiation, lower charge densities of Cl and Br relative to F, coupled by the higher degree of polymerization, which makes the incorporation of larger anions into the melt more difficult. More differentiated magmas have been predicted to have lower $D_F^{fluid/melt}$, based on the ability of F to replace hydroxyl and oxygen ions in minerals and substitute for O on the vertices of aluminate or silicate tetrahedral, meaning that it preferentially favors the melt relative to the fluid phase as magma becomes more silicic during differentiation (Dolejš and Baker 2007; Webster 1990). Our data help to confirm this inference (Fig. 7) by filling a compositional gap in pre-existing experimental data and demonstrating higher $D_F^{fluid/melt}$, i.e., more F partitioning into the fluid phase, in less-evolved magmas.

Contrary to the overall observation of high $D_{Cl}^{fluid/melt}$ and $D_{Br}^{fluid/melt}$ for the most differentiated magmas, within the Kelud data set we find negative correlations with respect to $D_{Cl}^{fluid/melt}$ and $D_{Br}^{fluid/melt}$ with differentiation (Fig. 6), which exist despite removing the concentration of halogens in the fluid as a factor. However, combining the Kelud and Quizapu data sets shows no significant effect of differentiation (Fig. 6), thus differentiation alone may not be able to explain the distribution of $D_{Cl}^{fluid/melt}$ and $D_{Br}^{fluid/melt}$ values. The compositional influence on partitioning may be more complex than mafic vs. felsic, but instead related to the availability of metal cations, which form ligand complexes with F, Cl, and Br. For instance, the negative correlation between differentiation with $D_{Cl}^{fluid/melt}$ and $D_{Br}^{fluid/melt}$ for the Kelud data set, which encompasses a larger range of compositions than Quizapu (Fig. 6), is likely controlled by Na, K, and Si complexes forming within these experimental melts (Online Materials[1] Figs. S5 and S6). Figure 7 combines both Quizapu and Kelud data sets and highlights the potential halogen complexes forming in all the experimental melts, by elements anti-correlated with $D^{fluid/melt}$ (e.g., K, Na, and Si for fluorine, Na and Ti for chlorine, and Ti bromine). The type of metal-ligand bonds that form (e.g., Na-Cl, K-Cl) can be related to both the similarity in their orbital energy and the Lewis acidity or basicity of the cation and anion pair.

The latter can be conceptualized following the bond valence model from Brown (2000), which uses ion charge and coordination number to provide bond strength indicators in valence units (v.u.) for individual ions, which correlates with electronegativity. For instance, cations and anions with similar bond strengths (e.g., Na^+ – 0.16 v.u., and Cl^- – 0.13 v.u.) and with the same number of atomic orbitals will be more likely to form strong associations, relative to cations that have larger bond strength differences, e.g., Cl^- with Ca^{2+} (0.27 v.u.) and less orbital overlap (e.g., K-Cl). These relationships are highlighted in the correlative plot in Figure 7, showing the Na^+ is anti-correlated with $D_{Cl}^{fluid/melt}$, whereas Ca^{2+} and K^+ are not. It is possible that some of the positive elemental correlations with $D^{fluid/melt}$ in Figure 7 may indicate preferential complexes forming within the aqueous fluid (e.g., KCl, CaF_2, KBr). The negative correlations between Ti and $D_{Cl}^{fluid/melt}$ and $D_{Br}^{fluid/melt}$ (Fig. 7) are not found in either Kelud or Quizapu data sets separately, unlike other elemental correlations (Online Materials[1] Figs. S5 and S6) and are therefore likely an artifact of bringing the two data sets together with inherently different Ti contents (Fig. 7). The strong association between Si and F in our experiments (Fig. 7) is explained by high silicon-fluorine bond strength, resulting from their high charge densities (e.g., Dolejš and Baker 2006; Dalou and Mysen 2015). Some studies suggest that halide complexes with Mg, Ca, and Al are also important (Webster et al. 2015), but this was not observed in our study. The strong elemental associations in the melt observed here (e.g., NaCl, SiF_4) are more consistent with in situ spectroscopic measurements (Dalou et al. 2015; Louvel et al. 2020).

The inclusion of other volatile species such as sulfur, may also affect $D_{Cl}^{fluid/melt}$ by altering the nature of the complexes that form (Webster et al. 2009; Beermann 2010). This effect seems to be dependent on the oxidation state, with $D_{Cl}^{fluid/melt}$ increasing with the addition of oxidized sulfur to the melts (Botcharnikov et al. 2004; Webster et al. 2003; Beermann 2010), due to the enhanced stabilization of Na, K, and Ca in S-bearing saline fluids. However, this effect is minimal at lower oxygen fugacities of NNO-0.5 (Zajacz et al. 2012). Sulfur concentrations were not measured here, but are likely be higher in the Quizapu samples, which evidenced by the presence of sulfide blebs visible under SEM (Ruprecht et al. 2012), compared to the Kelud samples where they were absent, and this may explain the different halide complexes formed in the melt [Na, K, and Si for Kelud (Online Materials[1] Fig. S5) and compared to Fe for Quizapu (Online Materials[1] Fig. S6)]. The reader is referred to Webster et al. (2020) for further discussion of the effect of oxidized vs. non-oxidized S on Cl solubility behavior.

The alumina-saturation index [molar $Al_2O_3/(Na_2O+K_2O+CaO)$] has been shown to influence halogen fluid/melt and crystal/melt partitioning behavior (e.g., Olin and Wolff 2012; Iveson et al. 2019), potentially accounting for some of the influence from these metal-ligand complexes (Fig. 8). Some broad trends of higher $D_{Br}^{fluid/melt}$ and lower $D_F^{fluid/melt}$ with increasing aluminosity exist, which can be attributed to the presence or absence of Na, K complexes. However, there is significant scatter, partly due to the combination of different *P-T* experimental conditions and partly because more elements than just Al, Na, K, and Ca are involved in the formation of melt halide complexes.

Effect of temperature

There are relatively few experiments that attempt to assess the influence of temperature on halogen partitioning. Most data suggest that temperature has a minor effect on Cl, relative to the much stronger controls of melt and fluid composition (Chevychelov et al. 2008; Stelling et al. 2008; Iveson et al. 2019). Bromine, however, may show stronger temperature dependence (Cadoux et al. 2018). Correlations between Cl, F, and Br fluid/melt partitioning and temperature are clearly evident in our experiments (Fig. 6); however, for the Quizapu data set this correlation is negative, with decreasing $D^{fluid/melt}$ values with increasing temperature, while the Kelud data set shows the opposite trend. Because the temperature (and pressure) of the experiment can also affect its melt composition through the crystallization or melting of mineral phases, it can be difficult to disentangle these two factors, especially because melt composition has a dominant role in controlling fluid/melt

partitioning. Certainly, for the Kelud experiments, the change in the melt composition is large (58–73 wt% SiO_2; Fig. 2), suggesting that the fluid/melt partitioning is most likely dominated by the change in melt composition, overprinting any temperature effect (Fig. 6). However, for the Quizapu experiments there is a relatively smaller compositional change in the melt chemistry (69–74 wt% SiO_2; Fig. 6). Therefore, the variation in experimental temperature (800–900 °C) likely explains the negative correlation of $D^{fluid/melt}$ observed for the Quizapu experiments. This concurs with the thermodynamic formulation from Thomas and Wood (2021) for anhydrous basalts, which also shows that Cl solubility in melt should increase with increasing temperature. This effect has been observed previously in experiments on Br partitioning, which show increasing $D_{Br}^{fluid/melt}$ with decreasing temperatures [900–1200 °C (Cadoux et al. 2018)]. The larger effect of temperature on $D_{Br}^{fluid/melt}$ compared to Cl (and especially F) may be related to the relatively weaker metal-ligand bonds formed by Br in the melt due to its lower electronegativity and charge density, relative to Cl and F. The smaller ionic size of F leads to larger lattice energies of fluorides and, therefore, higher temperature stability of F complexes, which may explain the smaller temperature effect on $D_F^{fluid/melt}$.

Effect of CO_2

Five H_2O+CO_2-bearing experiments (X_{H_2O} = 0.55) were conducted in this study and are compared with fluid/melt partitioning values for the same composition, pressure, and temperature conditions. The X_{H_2O} = 0.55 experiments follow similar compositional trends to those defined for X_{H_2O} = 1, suggesting that CO_2 did not have a strong influence on this trend (Fig. 6). In the Kelud data set, the X_{H_2O} = 0.55 experiments show generally lower $D_{Cl}^{fluid/melt}$; however, these were also more differentiated, and so the effect of melt composition may also be a factor here (Fig. 6). Other studies suggest that the effect of CO_2 on $D_{Cl}^{fluid/melt}$ partitioning is variable, studies of andesitic, phonolitic, and trachytic melts show that CO_2 in the fluid has little influence on $D_{Cl}^{fluid/melt}$ (Botcharnikov et al. 2006; Webster et al. 2014), while Alletti et al. (2009) observed decreasing values of $D_{Cl}^{fluid/melt}$ with increasing CO_2 in fluids coexisting with trachybasaltic melt at 25–100 MPa. Hsu et al. (2019) assessed the role of CO_2 systematically and found that CO_2 lowers $D_{Cl}^{fluid/melt}$. Following the empirical regression of Hsu et al. (2019) based on granitic melts, we found that this equation could not replicate the Cl partitioning values from our CO_2-H_2O experiments, although this seems to be calibrated for slightly higher pressures than the run conditions of our experiments. Our compilation (Fig. 8) suggests that average $D_{Cl}^{fluid/melt}$ for H_2O+CO_2-bearing experiments are lower than the pure H_2O experiments, but this is not outside the variation of their ranges. There is a limited data set of CO_2-bearing experiments to assess F and Br fluid/melt partitioning (Fig. 8); these data suggest that CO_2 addition has only a minor effect on $D_F^{fluid/melt}$ and $D_{Br}^{fluid/melt}$ when compared with other effects such as fluid and melt composition, but this effect may differ for higher fluid salinity than used in this study.

Implications

This study provides key information about halogen behavior in intermediate to silicic melts, compositions typical of those produced in subduction zone magmas, which have received far less study to date (Fig. 1), but commonly result in hazardous explosive eruptions and the generation of ores. Data across a wide range of compositions are required to build rigorous models of halogen behavior during volcanic processes. Using the approach outlined here of not doping experiments with halogens, but analyzing low concentrations with SIMS, opens up the potential for the measurement of halogens in previously conducted phase equilibria experiments. Our analysis supports the notion that melt composition has a strong control on Cl, F, and Br fluid/melt partitioning (e.g., Webster et al. 2018). Simple differentiation does not control the variation of partitioning values for Cl and Br partitioning (Fig. 6). Instead, particular elements (e.g., K, Al, Na) with an affinity to make complexes with Cl and Br in the melt can explain 40 to 60% of the variation in Br and Cl fluid/melt partition coefficients (Fig. 7). In contrast, F seems to favor the melt over the fluid with increasing differentiation, with >70% of the variation in $D_F^{fluid/melt}$ explained by Si concentration alone (Figs. 2 and 7). This observation may be applied to the interpretation of magmatic processes in melt inclusions and hydrous minerals (retrospectively), or volcanic gas monitoring (in real time). For instance, measurements of volcanic gas species are used to interpret changing depth of magma because H_2O, S, and CO_2 solubilities are particularly sensitive to pressure and oxidation state (e.g., de Moor et al. 2016). However, if S, H_2O, and CO_2 fluxes, and associated ratios remain constant, but halogen ratios such as (Cl+Br)/F ratios increase over time, this could point to differentiation, or even temperature changes of an underlying stationary magma reservoir (e.g., Aiuppa et al. 2002, 2007; Edmonds et al. 2003, 2009; Allard et al. 2005; Burton et al. 2007; Balcone-Boissard et al. 2010; Bobrowski and Giuffrida 2012; Christopher et al. 2015). The strong relationship of $D_F^{fluid/melt}$ with melt composition, which decreases both with differentiation (Fig. 6) and degree of aluminosity (Fig. 8), might also explain the higher extent of F degassing in basaltic and alkaline lava lakes relative to silicic stratovolcanoes; the former may be accentuated by gas exsolution in equilibrium at shallow pressures, <10 MPa (e.g., Edmonds et al. 2009; Oppenheimer et al. 2011). Individual magmatic volatile species are variably affected by different magmatic processes and conditions, such that by measuring a larger set of volatile species in melt inclusions, such as CO_2, H_2O, and S, along with F, Cl, and Br, one may be able to disentangle these magmatic conditions and processes prior to eruptions. For instance, trends toward higher (Cl+Br)/F melt ratios may indicate mafic injection due to the compositional effects, whereas trends to lower (Cl+Br)/F ratios, with increasing H_2O and relatively constant S, may point to differentiation of a stationary magma reservoir leading to second boiling. More fluid/melt partitioning data for a range of subduction zone magma compositions will also aid the calculation (e.g., via the melt inclusion petrological method) of Cl, F, and Br fluxes into the atmosphere for historical eruptions sourced from intermediate and silicic magmas, which have the potential for significant stratospheric ozone destruction (e.g., Kutterolf et al. 2013; Cadoux et al. 2015; Vidal et al. 2016).

Acknowledgments

Vitaly Chevchelov is thanked for the inclusion of compositional data. We thank Jon Wade and Phil Gopon for electron microprobe assistance and Richard Thomas and Bernie Wood for discussion. Thor Hansteen and an anonymous reviewer are thanked for their helpful comments to improve this paper.

Funding

M.C. acknowledges funding from NERC Independent Research fellowship NE/N014286/1. A.A.I. is currently funded by the Leverhulme Trust through an Early Career Fellowship. P.R. acknowledges funding from U.S. NSF grant EAR 1347880/1717288.

References cited

Aiuppa, A., Federico, C., Paonita, A., Pecoraino, G., and Valenza, M. (2002) S, Cl and F degassing as an indicator of volcanic dynamics: The 2001 eruption of Mount Etna. Geophysical Research Letters, 29, 1–4.

Aiuppa, A., Federico, C., Franco, A., Giudice, G., Gurrieri, S., Inguaggiato, S., Liuzzo, M., McGonigle, A.J.S., and Valenza, M. (2005) Emission of bromine and iodine from Mount Etna volcano. Geochemistry, Geophysics, Geosystems, 6, no. 8. 10.1029/2005gc000965

Aiuppa, A., Moretti, R., Federico, C., Giudice, G., Gurrieri, S., Liuzzo, M., Papale, P., Shinohara, H., and Valenza, M. (2007) Forecasting Etna eruptions by real-time observation of volcanic gas composition. Geology, 35, 1115–1118.

Aiuppa, A., Baker, D.R., and Webster, J.D. (2009) Halogens in volcanic systems. Chemical Geology, 263, 1–18.

Allard, P., Burton, M., and Mur, F. (2005) Spectroscopic evidence for a lava fountain driven by previously accumulated magmatic gas. Nature, 433, 407–410.

Alletti, M., Baker, D.R., Scaillet, B., Aiuppa, A., Moretti, R., and Ottolini, L. (2009) Chlorine partitioning between a basaltic melt and H_2O-CO_2 fluids at Mount Etna. Chemical Geology, 263, 37–50.

Alletti, M., Burgisser, A., Scaillet, B., and Oppenheimer, C. (2014) Chloride partitioning and solubility in hydrous phonolites from Erebus volcano: A contribution towards a multi-component degassing model. GeoResJ, 3-4, 27–45.

Baker, D.R., and Alletti, M. (2012) Fluid saturation and volatile partitioning between melts and hydrous fluids in crustal magmatic systems: The contribution of experimental measurements and solubility models. Earth-Science Reviews, 114, 298–324.

Balcone-Boissard, H., Villemant, B., and Boudon, G. (2010) Behavior of halogens during the degassing of felsic magmas. Geochemistry, Geophysics, Geosystems, 11.

Beermann, O. (2010) The solubility of sulfur and chlorine in H_2O-bearing dacites of Krakatau and basalts of Mt. Etna. Ph.D. thesis, Gottfried Wilhelm Leibniz Universität Hannover.

Beermann, O., Botcharnikov, R.E., and Nowak, M. (2015) Partitioning of sulfur and chlorine between aqueous fluid and basaltic melt at 1050 °C, 100 and 200 MPa. Chemical Geology, 418, 132–157.

Bell, A.S., and Simon, A. (2011) Experimental evidence for the alteration of the $Fe^{3+}/\Sigma Fe$ of silicate melt caused by the degassing of chlorine-bearing aqueous volatiles. Geology, 39, 499–502.

Bobrowski, N., and Giuffrida, G. (2012) Bromine monoxide/sulphur dioxide ratios in relation to volcanological observations at Mt. Etna 2006–2009. Solid Earth, 3, 433–445.

Bodnar, R.J., Lecumberri-Sanchez, P., Moncada, D., and Steele-MacInnis, M. (2013) Fluid inclusions in hydrothermal ore deposits. In K.K. Turekian and H.D. Holland, Eds., Treatise on Geochemistry, 2nd ed., p.119–142. Elsevier.

Borodulin, G.P., Chevychelov, V.Y., and Zaraysky, G.P. (2009) Experimental study of partitioning of tantalum, niobium, manganese, and fluorine between aqueous fluoride fluid and granitic and alkaline melts. Doklady Earth Sciences, 427, 868–873.

Botcharnikov, R.E., Behrens, H., Holtz, F., Koepke, J., and Sato, H. (2004) Sulfur and chlorine solubility in Mt. Unzen rhyodacitic melt at 850 °C and 200 MPa. Chemical Geology, 213(1–3), 207–225. doi: 10.1016/j.chemgeo.2004.08.044.

Botcharnikov, R.E., Behrens, H., and Holtz, F. (2006) Solubility and speciation of C-O-H fluids in andesitic melt at T = 1100–1300 °C and P = 200 and 500 MPa. Chemical Geology, 229, 125–143.

Botcharnikov, R.E., Holtz, F., and Behrens, H. (2015) Solubility and fluid-melt partitioning of H_2O and Cl in andesitic magmas as a function of pressure between 50 and 500 MPa. Chemical Geology, 418, 117–131.

Brown, I.D. (2000) The bond valence model as a tool for teaching inorganic chemistry: The ionic model revisited. Journal of Chemical Education, 77, 1070–1075.

Bureau, H., and Métrich, N. (2003) An experimental study of bromine behaviour in water-saturated silicic melts. Geochimica et Cosmochimica Acta, 67, 1689–1697.

Bureau, H., Keppler, H., and Métrich, N. (2000) Volcanic degassing of bromine and iodine: Experimental fluid/melt partitioning data and applications to stratospheric chemistry. Earth and Planetary Science Letters, 183, 51–60.

Bureau, H., Foy, E., Raepsaet, C., Somogyi, A., Munsch, P., Simon, G., and Kubsky, S. (2010) Bromine cycle in subduction zones through in situ Br monitoring in diamond anvil cells. Geochimica et Cosmochimica Acta, 74(13), 3839–3850. doi: 10.1016/j.gca.2010.04.001.

Burnham (1967) Hydrothermal fluids at the magmatic stage. In Geochemistry of Hydrothermal Ore Deposits, p. 34–76. Holt, Rinehart, and Winston.

Burton, M., Allard, P., Mure, F., and La Spina, A. (2007) Magmatic gas composition reveals the source depth of slug-driven strombolian explosive activity. Science, 317, 227–230.

Cadoux, A., Scaillet, B., Bekki, S., Oppenheimer, C., and Druitt, T.H. (2015) Stratospheric Ozone destruction by the Bronze-Age Minoan eruption (Santorini Volcano, Greece). Scientific Reports, 5, 12243–12212.

Cadoux, A., Iacono-Marziano, G., Scaillet, B., Aiuppa, A., Mather, T.A., Pyle, D.M., Deloule, E., Gennaro, E., and Paonita, A. (2018) The role of melt composition on aqueous fluid vs. silicate melt partitioning of bromine in magmas. Earth and Planetary Science Letters, 498, 450–463.

Cassidy, M., Castro, J.M., Helo, C., Troll, V.R., Deegan, F.M., Muir, D., Neave, D.A., and Mueller, S.P. (2016) Volatile dilution during magma injections and implications for volcano explosivity. Geology, 44, 1027–1030.

Cassidy, M., Ebmeier, S.K., Helo, C., Watt, S.F.L., Caudron, C., Odell, A., Spaans, K., Kristianto, P., Triastuty, H., Gunawan, H., and others (2019) Explosive eruptions with little warning: Experimental petrology and volcano monitoring observations from the 2014 eruption of Kelud, Indonesia. Geochemistry, Geophysics, Geosystems, 20, 4218–4247.

Chevychelov, V.Y. (2019) Partitioning of volatile components (Cl, F, and CO_2) in water-saturated fluid–magma systems of various composition. Petrology, 27, 585–605.

Chevychelov, V.Y., Bocharnikov, R.E., and Holtz, F. (2008) Experimental study of chlorine and fluorine partitioning between fluid and subalkaline basaltic melt. Doklady Earth Sciences, 422, 1089–1092.

Christopher, T.E., Blundy, J., Cashman, K., Cole, P., Edmonds, M., Smith, P.J., Sparks, R.S.J., and Stinton, A. (2015) Crustal-scale degassing due to magma system destabilization and magma-gas decoupling at Soufrière Hills Volcano, Montserrat. Geochemistry, Geophysics, Geosystems, 16, 2797–2811.

Cochain, B., Sanloup, C., de Grouchy, C., Crépisson, C., Bureau, H., Leroy, C., Kantor, I., and Irifune, T. (2015) Bromine speciation in hydrous silicate melts at high pressure. Chemical Geology, 404, 18–26.

Dalou, C., and Mysen, B.O. (2015) The effect of H_2O on F and Cl solubility and solution mechanisms of in aluminosilicate melts at high pressure and high temperature. American Mineralogist, 100, 633–643.

Dalou, C., Mysen, B.O., and Foustoukos, D. (2015) In-situ measurements of fluorine and chlorine speciation and partitioning between melts and aqueous fluids in the Na_2O-Al_2O_3-SiO_2-H_2O system. American Mineralogist, 100, 47–58.

Doherty, A.L., Webster, J.D., Goldoff, B.A., and Piccoli, P.M. (2014) Partitioning behavior of chlorine and fluorine in felsic melt–fluid(s)–apatite systems at 50 MPa and 850–950 °C. Chemical Geology, 384, 94–111.

Dolejš, D., and Baker, D.R. (2007) Liquidus equilibria in the system K_2O-Na_2O-Al_2O_3-SiO_2-F_2O-1-H_2O to 100 MPa: II. Differentiation paths of fluorosilicic magmas in hydrous systems. Journal of Petrology, 48, 807–828.

Dolejš, D., and Zajacz, Z. (2018) Halogens in silicic magmas and their hydrothermal systems. In D.E. Harlov and L. Aranovich, Eds., The Role of Halogens in Terrestrial and Extraterrestrial Geochemical Processes: Surface, Crust, and Mantle, pp 431–543. Springer.

Donovan, A., Tsanev, V., Oppenheimer, C., and Edmonds, M. (2014) Reactive halogens (BrO and OClO) detected in the plume of Soufrière Hills Volcano during an eruption hiatus. Geochemistry, Geophysics, Geosystems, 15, 3346–3363.

Edmonds, M., Herd, R.A., Galle, B., and Oppenheimer, C.M. (2003) Automated, high time-resolution measurements of SO_2 flux at Soufriere Hills Volcano, Montserrat. Bulletin of Volcanology, 65, 578–586.

Edmonds, M., Gerlach, T.M., and Herd, R.A. (2009) Halogen degassing during ascent and eruption of water-poor basaltic magma. Chemical Geology, 263, 122–130.

Erdmann, S., Martel, C., Pichavant, M., Bourdier, J.L., Champallier, R., Komorowski, J.C., and Cholik, N. (2016) Constraints from phase equilibrium experiments on pre-eruptive storage conditions in mixed magma systems: A case study on crystal-rich basaltic andesites from Mount Merapi, Indonesia. Journal of Petrology, 57, 535–560.

First, E.C., Hammer, J.E., Ruprecht, P., and Rutherford, M. (2021) Experimental constraints on dacite magma storage beneath Volcán Quizapu, Chile. Journal of Petrology, 62.

Gualda, G.A.R., and Ghiorso, M.S. (2015) MELTS-Excel: A Microsoft Excel-based MELTS interface for research and teaching of magma properties and evolution. Geochemistry, Geophysics, Geosystems, 16, 315–324.

Gutmann, A., Bobrowski, N., Roberts, T.J., Rüdiger, J., and Hoffmann, T. (2018) Advances in bromine speciation in volcanic plumes. Frontiers in Earth Science, 6, 1–24.

Hammer, J.E. (2008) Experimental studies of the kinetics and energetics of magma crystallization. Reviews in Mineralogy and Geochemistry, 69, 9–59.

Harlov, D.E., and Aranovich, L. (2018) The Role of Halogens in Terrestrial and Extraterrestrial Geochemical Processes: Surface, Crust, and Mantle, p 1030. Springer.

Hildreth, W., and Drake, R.E. (1992) Volcán Quizapu, Chilean Andes. Bulletin of Volcanology, 54, 93–125.

Hsu, Y.J., Zajacz, Z., Ulmer, P., and Heinrich, C.A. (2019) Chlorine partitioning between granitic melt and H_2O-CO_2-NaCl fluids in the Earth's upper crust and implications for magmatic-hydrothermal ore genesis. Geochimica et Cosmochimica Acta, 261, 171–190.

Iveson, A.A., Webster, J.D., Rowe, M.C., and Neill, O.K. (2017) Major element and halogen (F, Cl) mineral-melt-fluid partitioning in hydrous rhyodacitic melts at shallow crustal conditions. Journal of Petrology, 58, 2465–2492.

——— (2019) Fluid-melt trace-element partitioning behaviour between evolved melts and aqueous fluids: Experimental constraints on the magmatic-hydrothermal transport of metals. Chemical Geology, 516, 18–41.

Jeffery, A.J., Gertisser, R., Troll, V.R., Jolis, E.M., Dahren, B., Harris, C., Tindle, A.G., Preece, K., O'Driscoll, B., Humaida, H., Chadwick, J.P., and others (2013) The pre-eruptive magma plumbing system of the 2007–2008 dome-forming eruption

of Kelut volcano, East Java, Indonesia. Contributions to Mineralogy and Petrology, 166, 275–308.
Jochum, K.P., Stoll, B., Herwig, K., Willbold, M., Hofmann, A.W., Amini, M., Aarburg, S., Abouchami, W., Hellebrand, E., Mocek, B., and others (2006) MPI-DING reference glasses for in situ microanalysis: New reference values for element concentrations and isotope ratios. Geochemistry, Geophysics, Geosystems, 7.
Joyce, D.B., and Holloway, J.R. (1993) An experimental determination of the thermodynamic properties of H_2O-CO_2-NaCl fluids at high pressures and temperatures. Geochimica et Cosmochimica Acta, 57, 733–746.
Kendrick, M.A. (2012) High precision Cl, Br and I determinations in mineral standards using the noble gas method. Chemical Geology, 292-293, 116–126.
Kravchuk, I.F., and Keppler, H. (1994) Distribution of chloride between aqueous fluids and felsic melts at 2 kbar and 800 °C. European Journal of Mineralogy, 6(6), 913–923.
Kutterolf, S., Hansteen, T.H., Appel, K., Freundt, A., Krüger, K., Pérez, W., and Wehrmann, H. (2013) Combined bromine and chlorine release from large explosive volcanic eruptions: A threat to stratospheric ozone? Geology, 41, 707–710.
Louvel, M., Cadoux, A., Brooker, R.A., Proux, O., and Hazemann, J.L. (2020) New insights on Br speciation in volcanic glasses and structural controls on halogen degassing. American Mineralogist, 105, 795–780.
Lowenstern, J.B. (1994) Chlorine, fluid immiscibility, and degassing in peralkaline magmas from Pantelleria, Italy. American Mineralogist, 79, 353–369.
Marks, M.A.W., Wenzel, T., Whitehouse, M.J., Loose, M., Zack, T., Barth, M., Worgard, L., Krasz, V., Eby, G.N., Stosnach, H., and others (2012) The volatile inventory (F, Cl, Br, S, C) of magmatic apatite: An integrated analytical approach. Chemical Geology, 291, 241–255.
Marks, M.A.W., Kendrick, M.A., Eby, G.N., Zack, T., and Wenzel, T. (2017) The F, Cl, Br and I contents of Reference Glasses BHVO-2G, BIR-1G, BCR-2G, GSD-1G, GSE-1G, NIST SRM 610 and NIST SRM 612. Geostandards and Geoanalytical Research, 41, 107–122.
Matthews, W., Linnen, R.L., and Guo, Q. (2003) A filler-rod technique for controlling redox conditions in cold-seal pressure vessels. American Mineralogist, 88, 701–707.
Moor, J.M., Aiuppa, A., Avard, G., Wehrmann, H., Dunbar, N., Muller, C., Tamburello, G., Giudice, G., Liuzzo, M., Moretti, R., and others (2016) Turmoil at Turrialba Volcano (Costa Rica): Degassing and eruptive processes inferred from high-frequency gas monitoring. Journal of Geophysical Research: Solid Earth, 1–15.
Nielsen, C.H., and Sigurdsson, H. (1981) Quantitative methods for electron microprobe analysis of sodium in natural and synthetic glasses. American Mineralogist, 66(5-6), 547–552.
Olin, P.H., and Wolff, J.A. (2012) Partitioning of rare earth and high field strength elements between titanite and phonolitic liquid. Lithos, 128-131, 46–54.
Oppenheimer, C., Moretti, R., Kyle, P.R., Eschenbacher, A., Lowenstern, J.B., Hervig, R.L., and Dunbar, N.W. (2011) Mantle to surface degassing of alkalic magmas at Erebus volcano, Antarctica. Earth and Planetary Science Letters, 306, 261–271.
Papale, P., Moretti, R., and Barbato, D. (2006) The compositional dependence of the saturation surface of $H_2O + CO_2$ fluids in silicate melts. Chemical Geology, 229, 78–95.
Pichavant, M., Costa, F., Burgisser, A., Scaillet, B., Martel, C., and Poussineau, S. (2007) Equilibration scales in silicic to intermediate magmas—Implications for experimental studies. Journal of Petrology, 48, 1955–1972.
Pyle, D.M., and Mather, T.A. (2009) Halogens in igneous processes and their fluxes to the atmosphere and oceans from volcanic activity: A review. Chemical Geology, 263, 110–121.
Ruprecht, P., and Bachmann, O. (2010) Pre-eruptive reheating during magma mixing at Quizapu volcano and the implications for the explosiveness of silicic arc volcanoes. Geology, 38, 919–922.
Ruprecht, P., Bergantz, G.W., Cooper, K.M., and Hildreth, W. (2012) The crustal magma storage system of volcán Quizapu, Chile, and the effects of magma mixing on magma diversity. Journal of Petrology, 53, 801–840.
Shea, T., and Hammer, J.E. (2013) Oxidation in CSPV experiments involving H_2O-bearing mafic magmas: Quantification and mitigation. American Mineralogist, 98, 1285–1296. doi: 10.2138/am.2013.4253.
Shinohara, H. (2009) A missing link between volcanic degassing and experimental studies on chloride partitioning. Chemical Geology, 263, 51–59.
Signorelli, S., and Carroll, M.R. (2000) Solubility and fluid-melt partitioning of Cl in hydrous phonolitic melts. Geochimica et Cosmochimica Acta, 64(16), 2851–2862. doi: 10.1016/S0016-7037(00)00386-0.
Stelling, J., Botcharnikov, R.E., Beermann, O., and Nowak, M. (2008) Solubility of H_2O- and chlorine-bearing fluids in basaltic melt of Mount Etna at T = 1050–1250 °C and P = 200 MPa. Chemical Geology, 256, 102–109.
Tattitch, B., Chelle-Michou, C., Blundy, J., and Loucks, R.R. (2021) Chemical feedbacks during magma degassing control chlorine partitioning and metal extraction in volcanic arcs. Nature Communications, 12.
Teiber, H., Marks, M.A.W., Wenzel, T., Siebel, W., Altherr, R., and Markl, G. (2014) The distribution of halogens (F, Cl, Br) in granitoid rocks. Chemical Geology, 374-375, 92–109.
Thomas, R.W., and Wood, B.J. (2021) The chemical behaviour of chlorine in silicate melts. Geochimica et Cosmochimica Acta, 294, 28–42.
Vidal, C.M., Métrich, N., Komorowski, J.-C., Pratomo, I., Michel, A., Kartadinata, N., Robert, V., and Lavigne, F. (2016) The 1257 Samalas eruption (Lombok, Indonesia): The single greatest stratospheric gas release of the Common Era. Scientific Reports, 6, 34868.
Webster, J.D. (1990) Partitioning of F between H_2O and CO_2 fluids and topaz rhyolite melt—Implications for mineralizing magmatic-hydrothermal fluids in F-rich granitic systems. Contributions to Mineralogy and Petrology, 104, 424–438.
——— (1992) Water solubility and chlorine partitioning in Cl-rich granitic systems: Effects of melt composition at 2 kbar and 800 °C. Geochimica et Cosmochimica Acta, 56(2), 679–687. doi: 10.1016/0016-7037(92)90089-2
——— (1997) Exsolution of magmatic volatile phases from Cl-enriched mineralizing granitic magmas and implications for ore metal transport. Geochimica et Cosmochimica Acta, 61, 1017–1029.
Webster, J.D., and De Vivo, B. (2002) Experimental and modeled solubilities of chlorine in aluminosilicate melts, consequences of magma evolution, and implications for exsolution of hydrous chloride melt at Mt. Somma-Vesuvius. American Mineralogist, 87, 1046–1061.
Webster, J.D., and Holloway, J.R. (1990) Partitioning of F and Cl between magmatic hydrothermal fluids and highly evolved granitic magmas. In H.J. Stein and J.L. Hannah, Eds., Ore-bearing Granite Systems; Petrogenesis and Mineralizing Processes, 246. GSA Special Papers.
Webster, J.D., Kinzler, R.J., and Mathez, E.A. (1999) Chloride and water solubility in basalt and andesite melts and implications for magmatic degassing. Geochimica et Cosmochimica Acta, 63, 729–738.
Webster, J.D., De Vivo, B., and Tappen, C. (2003) Volatiles, magmatic degassing and eruptions of Mt. Somma-Vesuvius: constraints from silicate melt inclusions, Cl and H_2O solubility experiments and modeling. Developments in Volcanology, 5, 207–226.
Webster, J.D., Sintoni, M.F., and De Vivo, B. (2009) The partitioning behavior of Cl, S, and H_2O in aqueous vapor- ± saline-liquid saturated phonolitic and trachytic melts at 200 MPa, Chemical Geology, 263(1–4), 19–36. doi: 10.1016/j.chemgeo.2008.10.017.
Webster, J.D., Goldoff, B., Sintoni, M.F., Shimizu, N., and De Vivo, B. (2014) C-O-H-Cl-S-F volatile solubilities, partitioning, and mixing in phonolitic-trachytic melts and aqueous-carbonic vapor ± saline liquid at 200 MPa. Journal of Petrology, 55, 2217–2248.
Webster, J.D., Vetere, F., Botcharnikov, R.E., Goldoff, B., McBirney, A., and Doherty, A.L. (2015) Experimental and modeled chlorine solubilities in aluminosilicate melts at 1 to 7000 bars and 700 to 1250 °C: Applications to magmas of Augustine Volcano, Alaska. American Mineralogist, 100, 522–535.
Webster, J.D., Goldoff, B.A., Flesch, R.N., Nadeau, P.A., and Silbert, Z.W. (2017) Hydroxyl, Cl, and F partitioning between high-silica rhyolitic melts-apatite-fluid(s) at 50–200 MPa and 700–1000 °C. American Mineralogist, 102, 61–74.
Webster, J.D., Baker, D.R., and Aiuppa, A. (2018) Halogens in mafic and intermediate-silica content magmas. In D. Harlov and L. Aranovich, Eds., The Role of Halogens in Terrestrial and Extraterrestrial Geochemical Processes, p. 307–430. Springer.
Webster, J.D., Iveson, A.A., Rowe, M.C., and Webster, P.M. (2020) Chlorine and felsic magma evolution: Modeling the behavior of an under-appreciated volatile component. Geochimica et Cosmochimica Acta, 271, 248–288.
Zajacz, Z., Candela, P.A., Piccoli, P.M., and Sanchez-Valle, C. (2012) The partitioning of sulfur and chlorine between andesite melts and magmatic volatiles and the exchange coefficients of major cations. Geochimica et Cosmochimica Acta, 89, 81–101.

Manuscript received April 21, 2021
Manuscript accepted September 18, 2021
Manuscript handled by Justin Filiberto

Endnote:

[1]Deposit item AM-22-108109, Online Materials. Deposit items are free to all readers and found on the MSA website, via the specific issue's Table of Contents (go to http://www.minsocam.org/MSA/AmMin/TOC/2022/Oct2022_data/Oct2022_data.html).